

## THE SPITZER c2d SURVEY OF WEAK-LINE T TAURI STARS. II. NEW CONSTRAINTS ON THE TIMESCALE FOR PLANET BUILDING

LUCAS CIEZA,<sup>1</sup> DEBORAH L. PADGETT,<sup>2</sup> KARL R. STAPELFELDT,<sup>3</sup> JEAN-CHARLES AUGEREAU,<sup>4</sup> PAUL HARVEY,<sup>1</sup>  
NEAL J. EVANS, II,<sup>1</sup> BRUNO MERÍN,<sup>5</sup> DAVID KOERNER,<sup>6</sup> ANNEILA SARGENT,<sup>7</sup> EWINE F. VAN DISHOECK,<sup>8</sup>  
LORI ALLEN,<sup>9</sup> GEOFFREY BLAKE,<sup>7</sup> TIMOTHY BROOKE,<sup>7</sup> NICHOLAS CHAPMAN,<sup>10</sup>  
TRACY HUARD,<sup>9</sup> SHIH-PING LAI,<sup>10</sup> LEE MUNDY,<sup>10</sup> PHILIP C. MYERS,<sup>9</sup>  
WILLIAM SPIESMAN,<sup>1</sup> AND ZAHED WAHHAJ<sup>6</sup>

Received 2006 August 29; accepted 2007 May 29

### ABSTRACT

One of the central goals of the Spitzer Legacy Project “From Cores to Disks” (c2d) is to determine the frequency of circumstellar disks around weak-line T Tauri stars (WTTTs) and to study the properties and evolutionary status of these disks. Here we present a census of disks for a sample of over 230 WTTTs located in the c2d IRAC and MIPS maps of the Ophiuchus, Lupus, and Perseus Molecular Clouds. We find that  $\sim 20\%$  of the WTTTs in a magnitude-limited subsample have IR excesses at IRAC wavelengths. These disk frequencies are  $\sim 3$ –6 times larger than that recently found for a sample of relatively isolated WTTTs located outside the highest extinction regions covered by the c2d maps. The disk fractions we find are more consistent with those obtained in recent *Spitzer* studies of WTTTs in young clusters such as IC 348 and Tr 37. According to their location in the H-R diagram, the WTTTs with excesses in our sample are among the younger part of the age distribution. Still, up to  $\sim 50\%$  of the apparently youngest stars in the sample show no evidence of IR excess, suggesting that the circumstellar disks of a sizable fraction of pre-main-sequence stars dissipate in a timescale of  $\sim 1$  Myr. We also find that none of the stars in our sample apparently older than  $\sim 10$  Myr have detectable circumstellar disks at wavelengths  $< 24 \mu\text{m}$ . The WTTT disks in our sample exhibit a wide range of properties (SED morphology, inner radius,  $L_{\text{disk}}/L_*$ , etc.) that bridge the gaps observed between the CTTSs and the debris disk regimes.

*Subject headings:* infrared: stars — open clusters and associations: individual (IC 348) — planetary systems: protoplanetary disks — stars: pre-main-sequence

*Online material:* color figures, machine-readable tables

### 1. INTRODUCTION

Over the last couple of decades, it has been clearly established that circumstellar disks are an integral part of the star formation process. Even though there is currently no direct evidence that planets actually grow from circumstellar material, it has become increasingly clear that disks are potential birthplaces of planets because their masses, sizes, and compositions are consistent with those of the assumed preplanetary solar nebulae (Hillenbrand 2002). More recently, the discovery of exoplanets orbiting nearby main-sequence stars has confirmed that the formation of planets is a common process and not a rare phenomenon exclusive to the solar system.

Direct detection of forming planets is well beyond our current capabilities, and observing molecular hydrogen, which largely dominates the mass of primordial disks, is particularly challenging (Thi et al. 2001; Richter et al. 2002). However, the thermal emis-

sion from circumstellar dust is much easier to detect and study. For this reason, the study of the evolution of circumstellar dust has been a natural first step toward providing observational constraints on planet formation theories.

Strom et al. (1989) studied a sample of 83 classical T Tauri stars (CTTSs) and weak-line T Tauri stars (WTTTs) located in the Taurus-Auriga star-forming region in order to determine the fraction of objects with  $K$ -band ( $2.2 \mu\text{m}$ ) and *IRAS* excesses indicating the presence of a circumstellar disk. WTTTs are low-mass pre-main-sequence (PMS) stars that occupy the same region of the H-R diagram as CTTSs but do not show clear evidence of accretion. The distinction between the two is usually made based on the  $H\alpha$  equivalent width (EW). The  $H\alpha$  EW of CTTSs is  $> 10 \text{ \AA}$ , while the  $H\alpha$  EW of WTTTs is  $< 10 \text{ \AA}$ . Since there is a very strong correlation between spectroscopic signatures of gas accretion and the presence of near-IR excess (Hartigan et al. 1995), most CTTSs show near-IR excess while most WTTTs lack such an excess. Strom et al. (1989) found that 60% of their stars younger than 3 Myr showed a  $K$ -band excess, indicating the presence of a circumstellar disk, while only 10% of the stars older than 10 Myr did so. Based on these numbers, they estimated a disk dissipation timescale of  $< 3$ –10 Myr and claimed that their result was, at the time, “the best astrophysical constraint on the time available for planet building.” It has been argued that individual star-forming regions such as Taurus lack the intrinsic age spread necessary to investigate the dissipation timescale of circumstellar disks from individually derived ages (Hartmann 2001). However, similar disk lifetime studies based on the disk frequency of clusters with different mean ages and extending to the  $3.4 \mu\text{m}$   $L$  band (e.g., Haisch et al. 2001) have led to results similar to those presented

<sup>1</sup> Astronomy Department, University of Texas, Austin, TX 78712.

<sup>2</sup> Spitzer Science Center, California Institute of Technology, Pasadena, CA 91125.

<sup>3</sup> Jet Propulsion Laboratory, Pasadena, CA 91109.

<sup>4</sup> Laboratoire d’Astrophysique de Grenoble, BP 53, 38041 Grenoble Cedex 9, France.

<sup>5</sup> Leiden Observatory, 2300 RA Leiden, Netherlands; and Research and Scientific Support Department, ESTEC, European Space Agency, 2200 AG Noordwijk, Netherlands.

<sup>6</sup> Department of Physics and Astronomy, Northern Arizona University, Flagstaff, AZ 86011.

<sup>7</sup> California Institute of Technology, Pasadena, CA 91125.

<sup>8</sup> Leiden Observatory, 2300 RA Leiden, Netherlands.

<sup>9</sup> Smithsonian Astrophysical Observatory, Cambridge, MA 02138.

<sup>10</sup> Astronomy Department, University of Maryland, College Park, MD 20742.

by Strom and collaborators (for a review on the frequency of near-IR excesses based on a sample of  $\sim 3000$  PMS stars see Hillenbrand 2006). The  $K$ -band excess, when used as a disk indicator, is only sensitive to dust in the innermost part of the disk; therefore,  $K$ -band studies only constrain the dissipation timescale of a region of the disks that is much closer to the star than the locations corresponding to the orbits of any of the planets in the solar system (Mercury's semimajor axis is 0.39 AU). The dissipation timescale of the dust in the planet-forming regions might or might not be the same. Since the dynamical timescale is shorter and the surface density is higher closer to the central star, circumstellar disks are expected to evolve from the inside out. Most WTTSSs, which by definition present little or no evidence for accretion, also show little or no near-IR excess (Hartigan et al. 1995). However, even after the inner accretion disk has dissipated, it is entirely possible that WTTSSs still have enough material at larger radii to form terrestrial and giant planets. In fact, millimeter-wave observations show that at least 10% of WTTSSs have disks with estimated masses in the  $10^{-1}$  to  $10^{-3} M_{\odot}$  range (Osterloh & Beckwith 1995; Andrews & Williams 2005).

While the existence of planets around a significant fraction of all MS stars has been verified (e.g., Marcy & Butler 1998), the fundamentals of the planet formation process still remain open questions, especially for giant planets. There are currently three main theories for the formation of giant planets: core accretion, gravitational instability, and hybrid models that combine aspects of both theories. See Lissauer & Stevenson (2007) and Durisen et al. (2007) for two recent reviews of the core accretion and gravitational instability models and a discussion of the many outstanding questions.

Although it is unlikely that an observational estimate of the disk's dissipation timescale by itself can distinguish between the competing theoretical models mentioned above, estimates of the dissipation timescale of the planet-forming regions can impose valuable constraints on current theoretical models. In order to probe the planet-forming regions of disks around PMS stars, mid- and far-IR observations are required. Unfortunately, these spectral regions are not easily observable from the ground, and past space IR telescopes such as *IRAS* and the *Infrared Space Observatory (ISO)* were only sensitive enough to detect very bright optically thick disks in low-mass stars at the distance of nearest star-forming regions. These instruments lacked the sensitivity needed to detect the modest IR excesses expected for optically thin disks and faint optically thick disks. Thus, *Spitzer*'s sensitivity is required to establish whether most WTTSSs have optically thin disks, disks with inner holes, which are too cold to be detected in the near-IR from the ground, disks too faint to be detected by *IRAS* and *ISO*, or no disks at all. One of the main goals of the Spitzer Legacy Project "From Molecular Cores to Planet-forming Disks" (c2d; Evans et al. 2003) is to determine whether or not most WTTSSs have circumstellar disks and to characterize their properties and evolutionary status. Preliminary results from the c2d Legacy Project (Padgett et al. 2006, hereafter P06) showed that disks are rare ( $\sim 6\%$ ) among the population of WTTSSs distributed *around* nearby molecular clouds. However, other recent *Spitzer* studies have reported significantly larger disk fractions ( $\sim 30\%$ ) among WTTSSs in young clusters such as IC 348 and Tr 37 (Lada et al. 2006, hereafter L06; Sicilia-Aguilar et al. 2006). Here we study a sample of over 230 spectroscopically identified WTTSSs located in the c2d IRAC and MIPS maps of the Lupus, Ophiuchus, and Perseus Molecular Clouds in order to investigate the frequency of circumstellar disks as a function of stellar age. In § 2 we describe the c2d survey of molecular clouds and our sample of WTTSSs. In § 3 we identify IR excesses and investigate the properties of their

disks. In § 4 we compare our results to previous *Spitzer* results and discuss the evolutionary status of WTTSS disks. Also in § 4, we derive the ages of the WTTSSs in our sample from their location in the H-R diagram. We investigate the disk frequency as a function of stellar age and use our results to impose constraints on the timescale for planet building. Finally, our conclusions are summarized in § 5.

## 2. OBSERVATIONS

### 2.1. c2d Large Molecular Clouds and GTO Observations

As part of the c2d Legacy Project, *Spitzer* has mapped  $13.0 \text{ deg}^2$  of three nearby star-forming regions, Perseus, Ophiuchus, and Lupus, with IRAC (3.6, 4.5, 5.8, and  $8.0 \mu\text{m}$ ), and  $22.1 \text{ deg}^2$  with MIPS ( $24 \mu\text{m}$ ). MIPS 70 and  $160 \mu\text{m}$  observations were also taken, but due to sensitivity considerations, we do not include these observations in most of our analysis. The IRAC maps consist of two dithers of 10.4 s observations, each obtained at two epochs (41.6 s total) separated by several hours. The second-epoch observations were taken in the High Dynamic Range mode, which includes 0.4 s observations before the 10.4 s exposures, allowing photometry of both bright and faint stars at the same time. MIPS observations were taken with the fast scan mode, also in two different epochs of 15 s exposures each. See Jorgensen et al. (2006) and Young et al. (2005) for a detailed description of the observing strategy used for the c2d IRAC and MIPS survey of nearby molecular clouds.

In addition to the data from the c2d Legacy project, we use observations of IC 348 taken as part of the IRAC and MIPS Guaranteed Time Observer (GTO) programs (Program ID 36 and 58, respectively). The IRAC GTO observations cover a  $15' \times 15'$  field of view centered in the cluster and consist of two pairs of eight dithers of 96.8 s exposures for the 3.6, 4.5, and  $5.8 \mu\text{m}$  observations (e.g., 1549 s exposures per pixel). The  $8.0 \mu\text{m}$  observations consist of four pairs of eight dithers of 46.8 s exposures.<sup>11</sup> The MIPS  $24 \mu\text{m}$  GTO observations of IC 348 were taken in the medium scan mode, resulting in an average exposure time of  $80 \text{ s pixel}^{-1}$ . For consistency, we processed the basic calibrated data from the GTO programs and produced point-source catalogs using the c2d pipeline (Evans et al. 2005).<sup>12</sup> The c2d pipeline uses the c2d mosaicking/source extraction software c2dphot (Harvey et al. 2004), which is based on the mosaicking program MOPEX developed by the Spitzer Science Center, and the source extractor DoPHOT (Schechter et al. 1993).

Flux uncertainties in c2dphot are calculated in a standard way from a numerical estimate of the Hessian matrix (Press et al. 1992; Silvia 1996). This procedure for estimating uncertainties, although statistically correct, appears to underestimate the uncertainty as measured by the repeatability of flux measurements of the same objects at different epochs. For bright sources, there appears to be a random error floor to the best uncertainty possible with our observing techniques of 0.05 mag for the IRAC bands and 0.09 mag for the MIPS bands. The absolute calibration uncertainties are not included in our uncertainties. They are 5% and 10% for IRAC and MIPS, respectively (see data handbook for the instruments). As in most *Spitzer* surveys, the intrinsic sensitivity of the c2d observations is not uniform across the clouds due to variations in the total exposure time at different positions in the sky, in the amount of extended cloud emission, and in the

<sup>11</sup> The longest integration time of the  $8.0 \mu\text{m}$  array, nominally 100 s, consists of two exposures of 46.8 s each (see IRAC handbook, <http://ssc.spitzer.caltech.edu/irac/dh/>).

<sup>12</sup> See <http://ssc.spitzer.caltech.edu/legacy/>.

TABLE 1  
*Spitzer* DATA

ID	R.A. (J2000.0)	Decl. (J2000.0)	$F_{3.6}$ (mJy)	Error <sub>3.6</sub> (mJy)	$F_{4.5}$ (mJy)	Error <sub>4.5</sub> (mJy)	$F_{5.8}$ (mJy)	Error <sub>5.8</sub> (mJy)	$F_{8.0}$ (mJy)	Error <sub>8.0</sub> (mJy)	$F_{24}$ (mJy)	Error <sub>24</sub> (mJy)
IC 348-1 .....	55.8837	32.1048	1.06E+01	1.51E-01	7.09E+00	8.78E-02	4.81E+00	5.52E-02	2.79E+01	4.68E-02	...	...
IC 348-2 .....	55.8903	32.0293	4.96E+00	7.22E-02	3.42E+01	4.89E-02	2.52E+00	3.64E-02	1.42E+01	2.89E-02	...	...
IC 348-3 .....	55.9526	32.2308	3.23E+00	4.64E-02	2.39E+00	2.82E-02	1.65E+00	2.96E-02	9.38E-01	3.05E-02	...	...
IC 348-4 .....	55.9532	32.1259	9.01E+00	1.75E-01	6.51E+00	8.82E-02	4.13E+00	5.04E-02	2.34E+00	4.26E-02	...	...
IC 348-5 .....	55.9558	32.1778	7.47E+00	1.13E-01	5.55E+00	6.76E-02	3.57E+00	4.47E-02	2.13E+00	4.04E-02	...	...

NOTES.—Table 1 is published in its entirety in the electronic edition of the *Astrophysical Journal*. A portion is shown here for guidance regarding its form and content.

source confusion level. Based on the cumulative fraction of all sources detected in both epochs of the c2d observations, the overall 90% completeness levels of the c2d survey have been estimated to be 0.07, 0.12, 0.5, 0.4, and 1.0 mJy for 3.6, 4.5, 5.8, 8.0, and 24  $\mu$ m, respectively. See Evans et al. (2005) for a detailed discussion of the uncertainties and sensitivity limits of the c2d survey.

The IRAC observations are sensitive enough to allow robust detections of stellar photospheres in all four IRAC bands for our entire sample of WTTSSs in Ophiuchus and Lupus (distance  $\sim$ 125 pc and  $\sim$ 150–200 pc, respectively) and in  $\sim$ 85% of the objects in Perseus (distance  $\sim$ 320 pc). MIPS 24  $\mu$ m observations are not deep enough to reach the stellar photosphere of some low-mass objects (especially in Perseus, which is the most distant cloud we consider), but, in general, they are deep enough to detect optically thick disks in our entire sample. The different completeness levels of our disk census due to sensitivity considerations are discussed in more detail in § 3.1.1.

## 2.2. Sample Selection

The c2d maps contain several hundred young stars identified by their X-ray and H $\alpha$  brightness that have been spectroscopically classified as WTTSSs. Our sample was selected from the literature and is distributed as follows: 69 objects in Ophiuchus (Bouvier & Appenzeller 1992; Martin et al. 1998), 33 objects in Lupus (Hughes et al. 1994; Krautter et al. 1997), and 130 objects in Perseus (Luhman et al. 2003). The Lupus and Ophiuchus objects are distributed across the cloud maps, while the targets in Perseus are located exclusively in the IC 348 cluster. Of the 33 Lupus objects, 27 are located in the c2d maps of Lupus III and 6 lie within the c2d maps of Lupus I.

*Spitzer* spectral energy distributions (SEDs) of the WTTSSs in IC 348 have already been presented by L06. We include these objects in our sample because they increase the statistical significance of our results and allow us to compare a clustered population to the more distributed population of stars in Lupus and Ophiuchus. Also, we adopt a different disk identification criterion than L06, which results in a lower disk fraction than that obtained by the Lada group (see § 4.1.2). Furthermore, L06 adopt a single age

(2–3 Myr) for the stars in the IC 348 cluster and do not attempt to study the disk fraction as a function of age, which is one of the main goals of our paper.

All the objects in our sample, which are listed in Table 1, have known spectral types and small H $\alpha$  EWs. The spectral types are necessary to estimate stellar ages from the position of the targets in the H-R diagram and the contribution of the stellar photospheres to the observed SEDs, while the H $\alpha$  EWs are required to establish WTTSS status. The nominal division between CTTSs and WTTSSs is H $\alpha$  EW = 10 Å; however, since the H $\alpha$  EW due to chromospheric activity alone can reach this value for late M stars (e.g., Martin 1997), we have included in our study 18 M2–M7 stars (<8% of our sample) with H $\alpha$  EW up to 15 Å. Also,  $\sim$ 8% of the stars in our sample show H $\alpha$  in absorption rather than in emission.

We note that even though there is a strong correlation between H $\alpha$  emission and other accretion signatures such as optical veiling, a single-epoch low-resolution measurement of H $\alpha$  equivalent width is not enough to rule out active accretion for at least two reasons. First, even when a narrow range of spectral types is considered, the distribution of H $\alpha$  EWs of T Tauri stars does not show a clear gap between accreting and nonaccreting objects (e.g., the H $\alpha$  EWs of weakly accreting PMS stars overlap with those of chromospherically active nonaccreting stars). Second, accretion itself is a highly variable process, and some objects constantly move across the WTTSS-CTTS H $\alpha$  EW boundary. Therefore, we consider our sample to be composed of mostly nonaccreting objects but do not rule out the presence of some actively accreting interlopers.

## 2.3. Complementary Data

In order to construct more complete SEDs of our WTTSSs, we have collected the Two Micron All Sky Survey (2MASS) photometry for our entire sample and the  $V$ -,  $R_C$ -, and  $I_C$ -band photometry reported by Hughes et al. (1994) and Wichmann et al. (1997) for 24 of our 33 Lupus objects. Also we have obtained our own  $VR_CI_C$  optical observations for 52 of our 69 Ophiuchus targets and  $R_C$ - and  $I_C$ -band observations for 115 of the 130 objects

TABLE 2  
NON-*Spitzer* DATA

ID	R.A. (J2000.0)	Decl. (J2000.0)	Spectral Type	H $\alpha$ (Å)	$V$ (mag)	Error <sub><math>V</math></sub> (mag)	$R_C$ (mag)	Error <sub><math>R_C</math></sub> (mag)	$I_C$ (mag)	Error <sub><math>I_C</math></sub> (mag)	$J$ (mag)	$H$ (mag)	$K_s$ (mag)
IC 348-1 .....	55.8837	32.1048	M0.75	1.0	...	...	14.81	0.03	13.73	0.03	12.18	11.38	11.13
IC 348-2 .....	55.8903	32.0293	M5	5.0	...	...	17.93	0.03	15.91	0.03	13.36	12.57	12.22
IC 348-3 .....	55.9526	32.2308	M5	6	...	...	17.92	0.03	16.05	0.03	13.59	12.98	12.64
IC 348-4 .....	55.9532	32.1259	M1.5	0	...	...	15.44	0.03	14.16	0.03	12.44	11.59	11.34
IC 348-5 .....	55.9558	32.1778	M3.5	11	...	...	16.36	0.03	14.76	0.03	12.58	11.80	11.54

NOTES.—Table 2 is published in its entirety in the electronic edition of the *Astrophysical Journal*. A portion is shown here for guidance regarding its form and content.

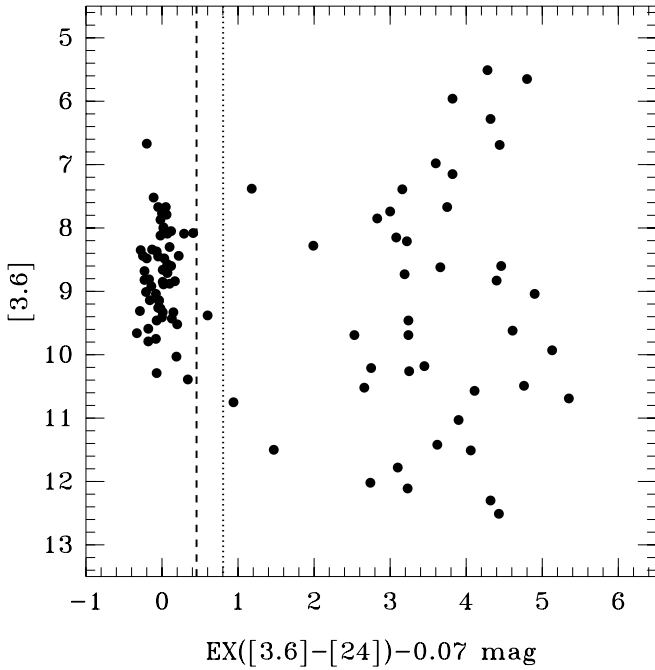


FIG. 1a

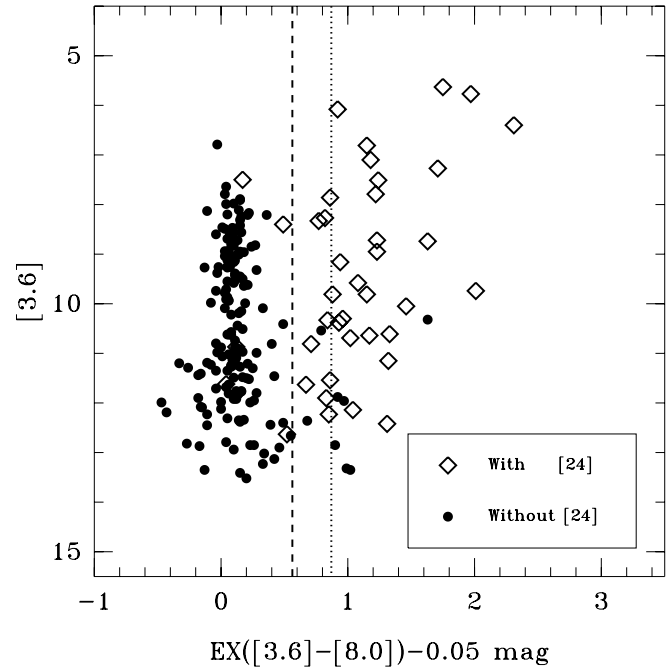


FIG. 1b

FIG. 1.—(a) [3.6] vs. EX([3.6] – [24]) and (b) [3.6] vs. EX([3.6] – [8.0]) diagrams for our sample of WTTs used for disk identification. See text for definitions. The 3 and 5  $\sigma$  dispersions of the stellar photospheres are shown as dashed and dotted lines, respectively. Most of the disks are detected at 24  $\mu\text{m}$ .

in IC 348 with the 0.8 m telescope at McDonald Observatory. The Ophiuchus targets were observed in seven different 46.2'  $\times$  46.2' fields of view during the photometric nights of 2005 June 20–21 with exposures times of 30, 50, and 100 s for the  $V$ ,  $R_C$ , and  $I_C$  bands, respectively. The objects in IC 348 were observed in a single field of view with 200 and 150 s exposures in the  $R_C$  and  $I_C$  bands, respectively. In addition to the program stars, on each night, three fields of Landolt standards ( $\sim$ 5 standards per field) were observed at different air masses. The seeing ranged from 1.5'' to 2'' when the observations were made. We reduced the data and performed aperture photometry using the standard IRAF packages CCDRED and DAOPHOT. We used a 5.4'' (4 pixel) aperture and a sky annulus with inner and outer radii of 16.2'' and 22.95'', respectively.

The rms scatter of the photometric solutions applied to the programs stars was  $<0.02$  mag in all three filters. We adopt a conservative *minimum* photometric error of 0.03 mag. We report the magnitudes and the uncertainties for all the objects with estimated photometric error less than  $\sim 0.2$  mag. The *Spitzer* photometry for our entire sample is listed in Table 1. The non-*Spitzer* data—optical and 2MASS photometry, along with the spectral types and H $\alpha$  equivalent widths from the literature—are listed in Table 2.

### 3. RESULTS

#### 3.1. Disk Identification

In order to identify the stars with disks, we compare the extinction-corrected *Spitzer* colors of our targets to those predicted by NextGen models (Hauschildt et al. 1999), convolved with the *Spitzer* bandpasses, for the photospheres of stars of the corresponding spectral types. The broader the wavelength baseline of the color used, the larger is the expected excess of the stars with disks; therefore, the available color that provides the most clear disk identification is [3.6] – [24]. However, since

both *Spitzer*'s sensitivity and the photospheric fluxes decrease with increasing wavelength, not all sources are detected at wavelengths longer than 5.8  $\mu\text{m}$ .

In Figure 1a we plot [3.6] versus EX([3.6] – [24]), for the 98 stars with 3.6 and 24  $\mu\text{m}$  fluxes available, where EX([3.6] – [24]) is  $([3.6] - [24])_{\text{obs},o} - ([3.6] - [24])_{\text{model}}$ ,  $([3.6] - [24])_{\text{obs},o}$  are the observed colors corrected for extinction, and  $([3.6] - [24])_{\text{model}}$  are the photospheric colors predicted by the NextGen models. We estimate the extinction,  $A_V$ , using  $A_V = 4.76(E(R-I) = 4.76[(R_C - I_C)_{\text{obs}} - (R_C - I_C)_o])$ . The intrinsic stellar colors,  $(R_C - I_C)_o$ , come from Kenyon & Hartmann (1995). For objects without  $R_C$  and  $I_C$  fluxes available, we use  $A_V = 5.88(E(J-K_s))$ .

TABLE 3  
ADOPTED EXTINCTION RELATIONS

Band	$\lambda$ ( $\mu\text{m}$ )	$A_V/A_\lambda^{\text{a}}$
$V$ .....	0.55	1.00
$R_C$ .....	0.65	0.79
$I_C$ .....	0.80	0.58
$J$ .....	1.25	0.26
$H$ .....	1.66	0.15
$K_s$ .....	2.2	0.09
IRAC-1.....	3.6	0.04
IRAC-2.....	4.5	0.03
IRAC-3.....	5.8	0.02
IRAC-4.....	8.0	0.01
MIPS-1 .....	24	0.002

<sup>a</sup> The extinction relations for the optical and 2MASS wavelengths come from the Asiago database of photometric systems (<http://ulisse.pd.astro.it/Astro/ADPS/enter.html>; Fiorucci & Munari 2003), while those for the *Spitzer* bands come from T. Huard et al. (2007, in preparation).

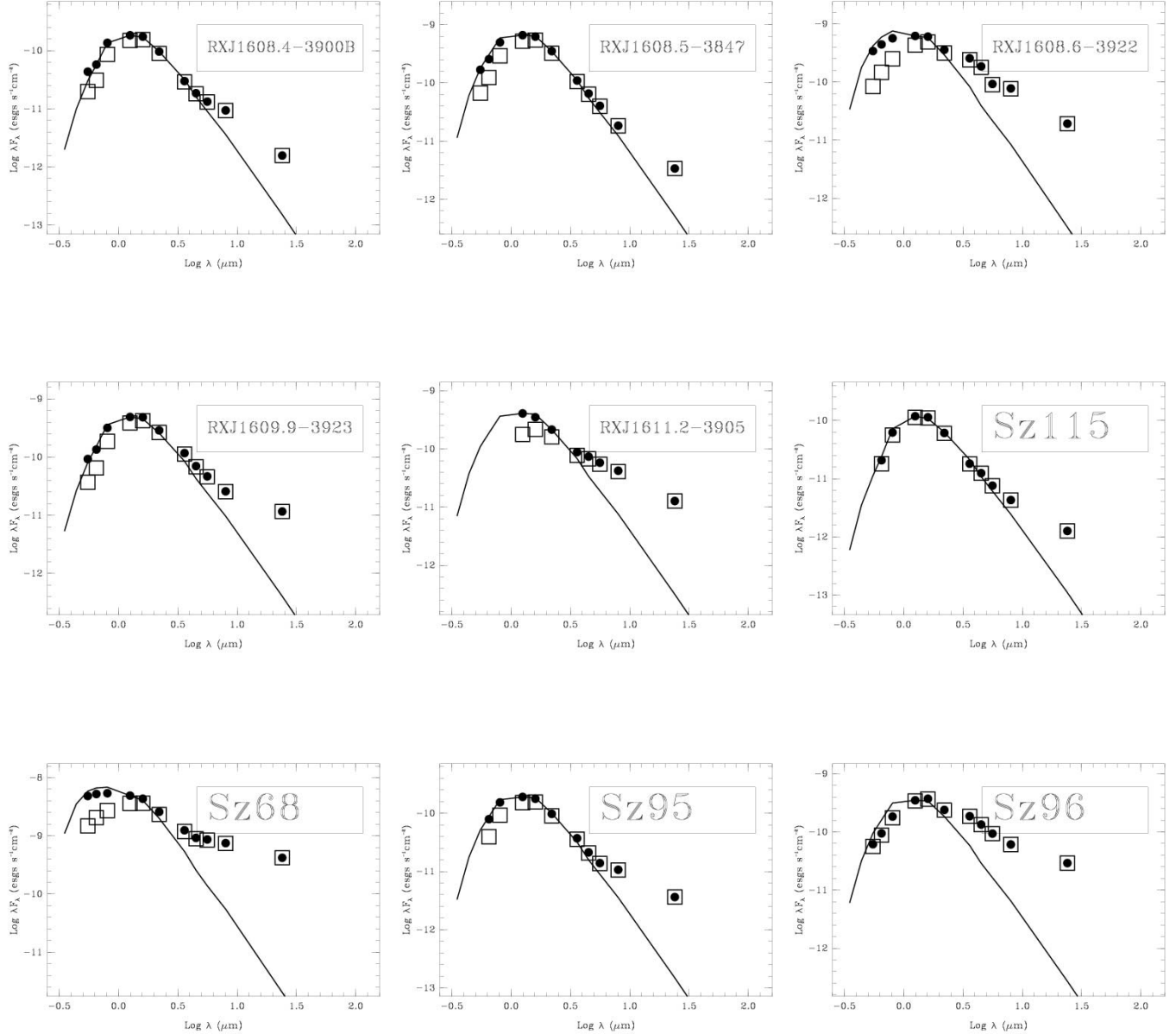


FIG. 2.—SEDs of WTTS disks in Lupus. The open squares represent the observed optical, 2MASS, IRAC, and MIPS 24  $\mu\text{m}$  fluxes, while the filled circles correspond to the extinction-corrected values. Model photospheres corresponding to published spectral types are shown for comparison.

We note that this will result in an overestimated extinction for objects with significant  $K$ -band excess. The extinction at 8 and 24  $\mu\text{m}$  is calculated according to Table 3.

We consider objects with  $[3.6] - [24] < 0.7$  to be those without excess whose emission arises solely from the stellar photosphere. The mean  $\text{EX}([3.6] - [24])$  value for this group is not zero but 0.07 mag with a 1  $\sigma$  dispersion of 0.17 mag. The 0.07 mag offset of the observed stellar photospheres with respect to the models is probably due to a combination of the systematic errors in the absolute flux calibrations, the stellar models, and the extinction corrections. In Figure 1a we treat this offset by subtracting 0.07 mag from all the  $\text{EX}([3.6] - [24])$  values. We find that 40 objects have a  $[3.6] - [24]$  excess larger than 5  $\sigma$ . These are very robust disk identifications. One object, RX J1622.6-2345, has  $[3.6] - [24]$  excess just over 3  $\sigma$ . We consider this object to be a good disk candidate, but we warn the reader of its lower significance. Since the c2d MIPS maps cover a larger area than the IRAC maps, 24  $\mu\text{m}$  is the only *Spitzer* flux available for

five stars in our sample. In these cases, we use  $[K] - [24]$  colors for disk identification. None of the five objects for which MIPS 24  $\mu\text{m}$  is the only available *Spitzer* flux show a significant  $K - 24 \mu\text{m}$  excess. Of the 127 stars without measured  $[3.6] - [24]$  or  $[K] - [24]$  colors, 112 have  $[3.6] - [8.0]$  colors available. Figure 1b is analogous to Figure 1a, but here we plot  $[3.6]$  versus  $\text{EX}([3.6] - [8.0])$  for all the stars with measured  $[3.6] - [8.0]$  colors, including the ones from Figure 1a, which are shown as open diamonds. Following Cieza & Baliber (2006), objects with  $[3.6] - [8.0] < 0.7$  are considered stellar photospheres. In this case, the mean color offset with respect to the models is 0.05 mag. The standard deviation of the stellar photospheres is 0.16 mag, but the error clearly increases with decreasing brightness. We find that only six objects not detected at 24  $\mu\text{m}$  show clear evidence ( $>5 \sigma$ ) for 8  $\mu\text{m}$  excess. Two objects, IC 348-76 and IC 348-67, show excesses between 3 and 5  $\sigma$ . Since the SEDs of these two objects show a hint of IR excess at 4.5 and 5.8  $\mu\text{m}$ , we consider these two objects to be good disk candidates. We find that none of the 15 objects without

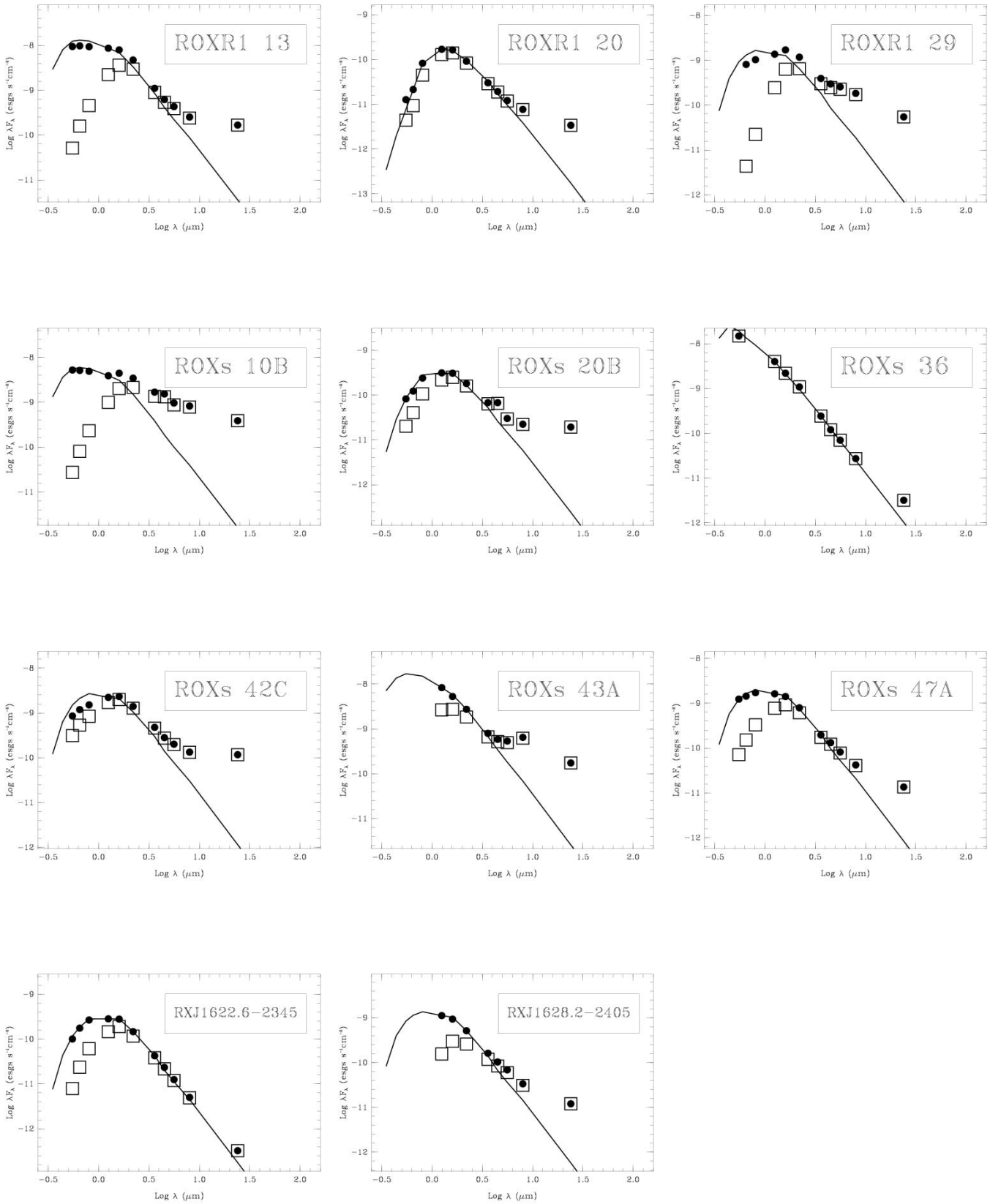


FIG. 3.—SEDs of WTTS disks in Ophiuchus.

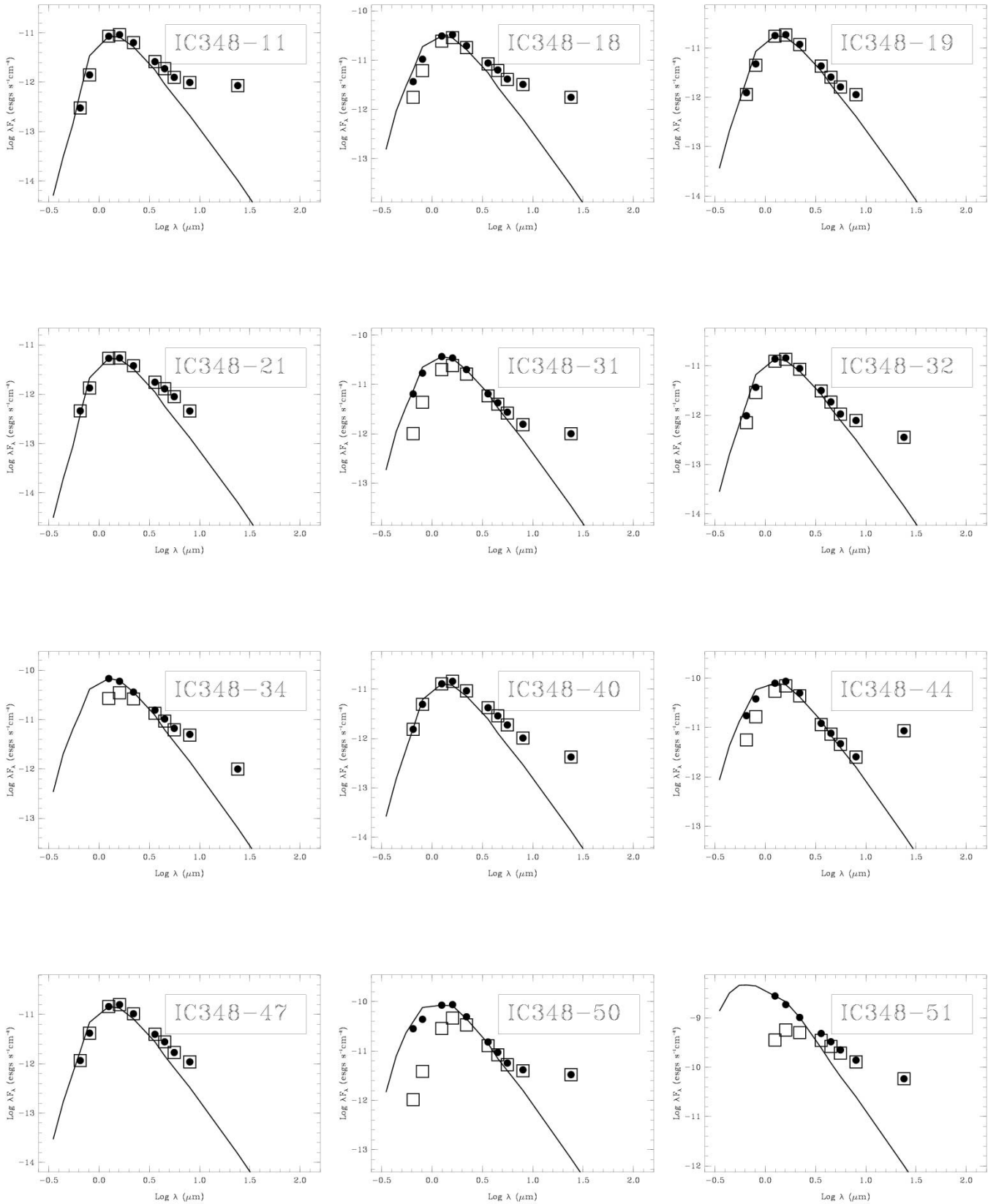


FIG. 4.—SEDs of WTTS disks in IC 348.

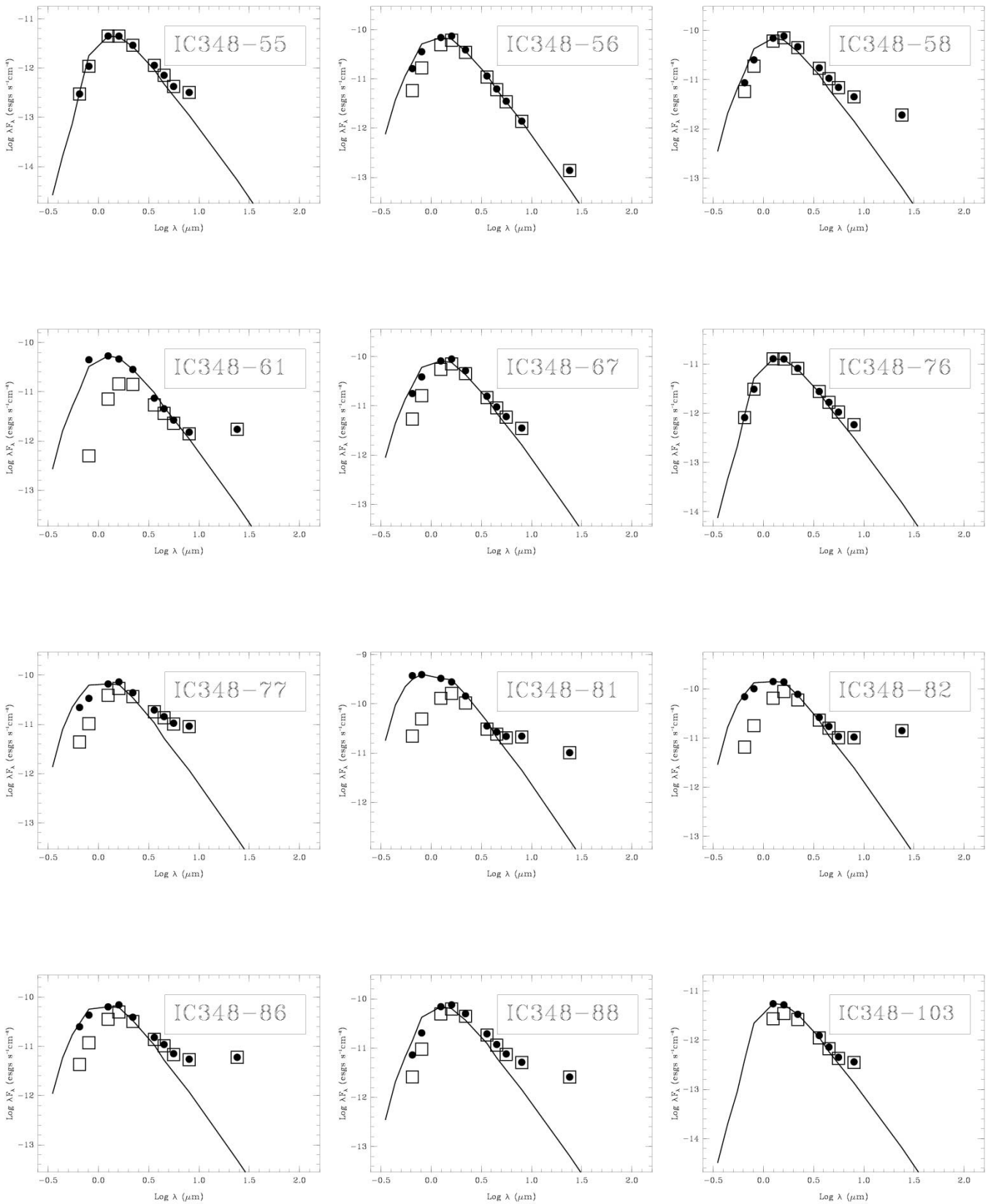


FIG. 4.—Continued

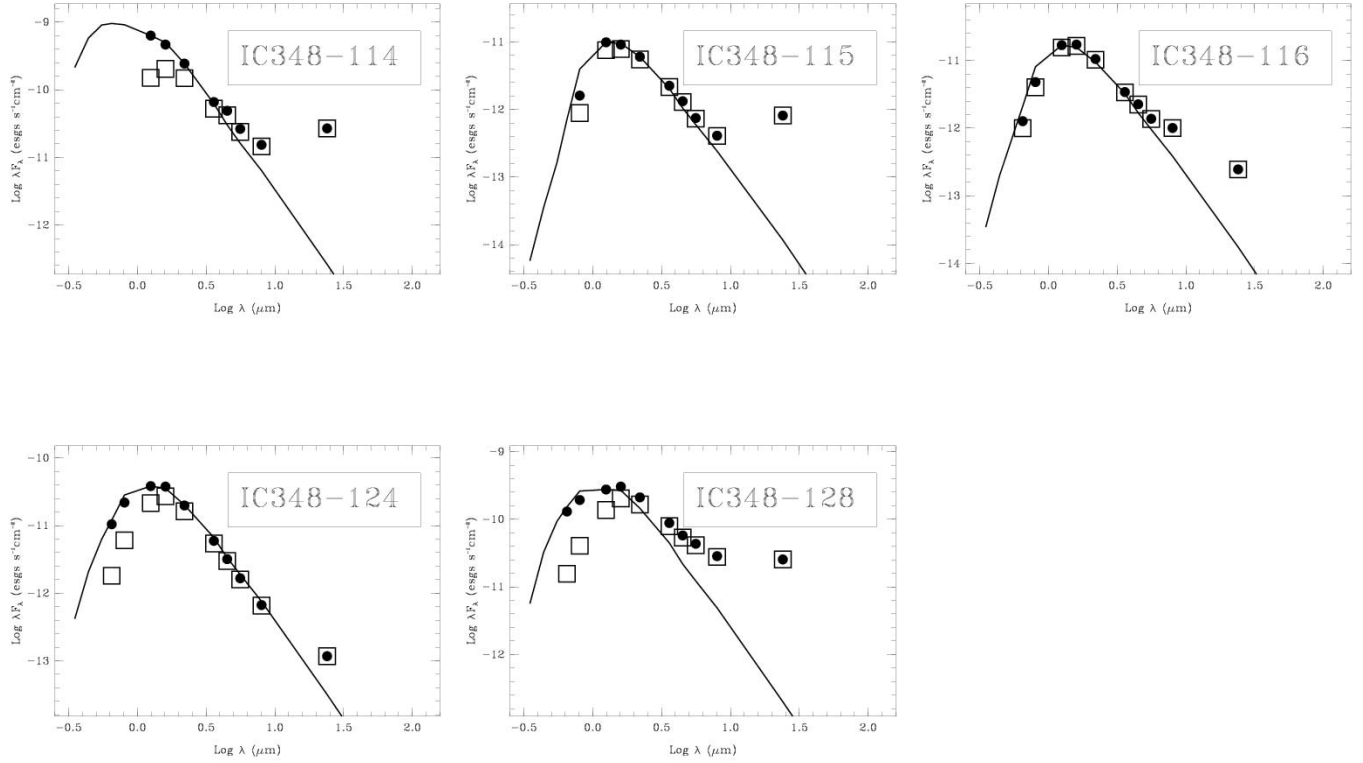


FIG. 4.—Continued

$[3.6] - [24]$ ,  $[K_s] - [24]$ , or  $[3.6] - [8.0]$  colors available show a significant  $[3.6] - [5.8]$  excess.

The SEDs of the WTTs disks in Lupus, Ophiuchus, and IC 348 are shown in Figures 2, 3, and 4, respectively. The open squares represent the observed optical, 2MASS, IRAC, and MIPS 24  $\mu\text{m}$  fluxes, while the filled circles correspond to the extinction-corrected values. The  $A_V$  values are estimated as described above for Figure 1, while the extinctions at other wavelengths are calculated according to Table 3. NextGen model photospheres, corresponding to published spectral types and normalized to the extinction-corrected  $J$  band, are shown for comparison.

### 3.1.1. Disk Census Completeness

Following the procedure described above, we identify a total of 46 WTTs disks and three disk candidates. For definiteness, we consider these three disk candidates to be real in the rest of the paper. However, we note that the completeness of our disk census is lower for our IC 348 sample than it is for the sample of Lupus and Ophiuchus WTTs.

The IRAC observations are sensitive enough to allow robust detections of stellar photospheres in all four IRAC bands for WTTs in the sample from Lupus and Ophiuchus (102 objects in total). Also, the five objects in Lupus and Ophiuchus that fall outside the c2d IRAC maps all have 24  $\mu\text{m}$  fluxes consistent with stellar photospheres, which rules out the presence of any significant IRAC excess in these objects. Therefore, the census of IRAC excesses in our sample of Lupus and Ophiuchus WTTs is likely to be complete (i.e., only 17 out of the 102 WTTs in Lupus and Ophiuchus have significant IRAC excesses). At 24  $\mu\text{m}$ , we detect<sup>13</sup>

80% (82/102) of the Lupus and Ophiuchus objects. Thus, it is possible that some of the 20 WTTs from the Lupus and Ophiuchus sample that are not detected at 24  $\mu\text{m}$  have SEDs that start to diverge from their photospheres longward of 8.0  $\mu\text{m}$  but remain below our sensitivity at 24  $\mu\text{m}$ . We find that all the objects with IRAC excess are detected at 24  $\mu\text{m}$  and that only 2 of the 82 objects detected at 24  $\mu\text{m}$  have excesses that only become evident at this wavelength.

In our IC 348 sample, 11% (14/130) of the objects are not detected at 8.0  $\mu\text{m}$  and 82% (107/130) are not detected at 24  $\mu\text{m}$ . The longer integration times of the GTO IRAC observations of IC 348 with respect to the c2d observation of Lupus and Ophiuchus (1548 s vs. 46.8 s) more than compensate the effect of the distance (320 pc vs. 125–200 pc) on the expected sensitivities. However, the high background of the IC 348 cluster becomes the limiting factor for the detection of faint sources at 8.0  $\mu\text{m}$ . At 24  $\mu\text{m}$ , the depth of the GTO observations only partially compensates for the greater distance of IC 348, and the effect of the background becomes even larger than it is at 8.0  $\mu\text{m}$ . The combination of these two factors explains the very low detection rate of IC 348 members at 24  $\mu\text{m}$ . None of the 14 objects without an 8.0 or 24  $\mu\text{m}$  detection show a significant 5.8  $\mu\text{m}$  excess that would indicate the presence of circumstellar disks. However, some of these 14 WTTs could have SEDs that start to diverge from their photospheres longward of 5.8  $\mu\text{m}$  but remain below our sensitivity at 8.0 and 24  $\mu\text{m}$ . Finally, we find that 91% (21/23) of the objects detected at 24  $\mu\text{m}$  also show significant IRAC excesses, which is consistent with the results for Lupus and Ophiuchus. Obviously, in IC 348, we are likely to have missed most of the stars for which the onset of the IR excess occurs longward of 8.0  $\mu\text{m}$ .

### 3.1.2. Disk Fraction Statistics

<sup>13</sup> By “detect” we mean that the flux of the object has been measured regardless of whether or not the star has an excess. All the objects have been observed at 24  $\mu\text{m}$ ; therefore, a nondetection implies that the flux of the object is below our 24  $\mu\text{m}$  sensitivity limit.

In § 3.1 we tried to present a disk census as complete as possible given the available data. However, since the sensitivity of

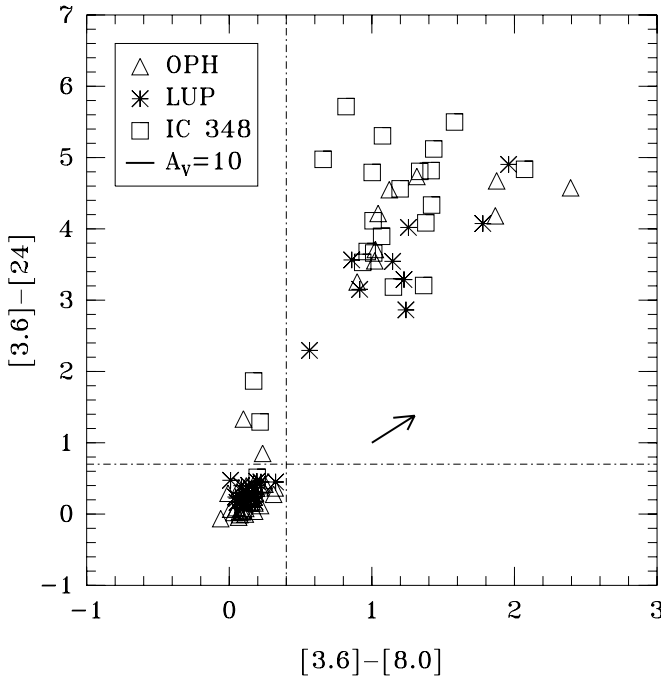


FIG. 5a

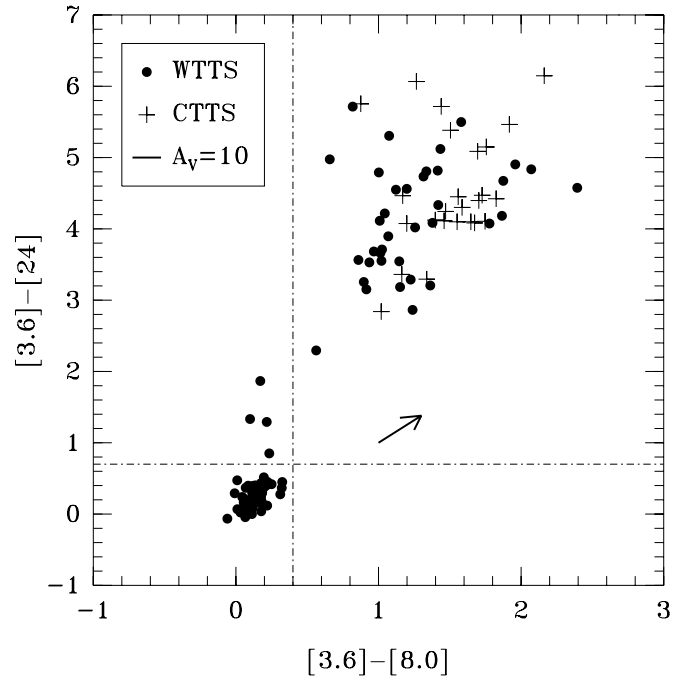


FIG. 5b

FIG. 5.—(a)  $[3.6] - [24]$  vs.  $[3.6] - [8.0]$  colors of our sample of WTTS stars. Based on this diagram, we identify three different groups: (1) stellar photosphere with  $[3.6] - [24] < 0.7$  and  $[3.6] - [8.0] < 0.4$ , (2) objects with  $[3.6] - [24] > 0.7$  and  $[3.6] - [8.0] < 0.4$  that show significant  $24\text{ }\mu\text{m}$  excess but no evidence for  $8.0\text{ }\mu\text{m}$  excess, and (3) objects with  $[3.6] - [24] > 0.7$  and  $[3.6] - [8.0] > 0.4$  that show evidence for both IRAC and MIPS excesses. Objects in the second group are likely to have optically thin disks (see § 3.2.4). (b) Combination of our sample of WTTSs with a sample of CTTTs from Hartmann et al. (2005) and L06.

our disk survey is not uniform across all wavelengths and varies from region to region due to distance and background level effects, we derive disk fraction statistics from the number of objects with excess at IRAC wavelengths (IRAC disk fraction, hereafter) in a magnitude-limited subsample that is not likely to be affected by sensitivity variations.

As discussed in the previous section, we consider our census of IRAC excesses in our sample of Lupus and Ophiuchus WTTSs to be complete. Excluding the disks that are only detected longward of  $10\text{ }\mu\text{m}$  (ROXs 36 and RX J1622.6–2345), we derive the following IRAC disk fractions:  $27\% \pm 7\%$  (9/33) for Lupus and  $13\% \pm 4\%$  (9/69) for Ophiuchus. For IC 348, we restrict our sample to the 96 objects with  $3.6\text{ }\mu\text{m}$  fluxes greater than  $3.2\text{ mJy}$ , a level above which we also detect at  $8.0\text{ }\mu\text{m}$  every object in our sample. We find that 22 of these 96 objects show significant IRAC excess, which leads to a disk fraction of  $23\% \pm 4\%$ . Combining the objects in Lupus, Ophiuchus, and IC 348, we derive an overall IRAC disk fraction of  $20\% \pm 3\%$  (40/198). The IRAC disk fractions of WTTSs in Lupus and Ophiuchus bracket that of the IC 348 cluster. This suggests that the disk fraction in IC 348 WTTS targets is not strongly affected by the cluster environment.

At  $24\text{ }\mu\text{m}$ , the sensitivity of our survey is significantly less uniform than at IRAC wavelengths. We find that even some of our brightest objects lack  $24\text{ }\mu\text{m}$  detections due to the strong background emission surrounding them. This prevents us from deriving robust MIPS disk fraction statistics even from a magnitude-limited subsample.

### 3.2. Disk Properties

#### 3.2.1. Selected Color-Color Diagrams

In this section we place our sample of WTTSs in *Spitzer* color-color diagrams as our first attempt to explore the diversity of

WTTS disks. For comparison, we also include in these diagrams two samples of 83 and 66 CTTTs from Taurus and IC 348, respectively. We used the  $\text{H}\alpha$  EW from Luhman et al. (2003) to select the sample of CTTTs in IC 348. For these objects we use our own photometry. The *Spitzer* fluxes of the Taurus CTTTs come from Hartmann et al. (2005). In Figures 5 and 6 we show an  $A_V = 10$  extinction vector based on Table 3; however, we note that for most of the stars in our sample the extinction is *significantly* smaller. The mean  $A_V$  we derive for our Lupus, Ophiuchus, and IC 348 WTTS samples are 0.64, 2.7, and 1.7 mag, respectively. Also, 93% of our sample has  $A_V < 5$  mag, and the remaining 7% has  $10\text{ mag} < A_V < 5\text{ mag}$ .

Figure 5a shows the  $[3.6] - [24]$  versus  $[3.6] - [8.0]$  colors of our sample of WTTSs. Based on the colors shown, we identify three different groups. The first group consists of objects with  $[3.6] - [24] < 0.7$  and  $[3.6] - [8.0] < 0.4$ , which are consistent with bare stellar photospheres. The second group consists of stars with  $[3.6] - [24] > 0.7$  and  $[3.6] - [8.0] < 0.4$  (i.e., their SEDs start to diverge from their stellar photospheres longward of  $8.0\text{ }\mu\text{m}$ ). The four stars in this group are RX J1622.6–2345, ROXs 36, IC 348-56, and IC 348-124. In § 3.2.4 we find that the objects in this second group have the lowest fractional disk luminosities of the sample. In fact, all four objects have  $L_{\text{disk}}/L_* < 10^{-3}$ , which suggests the presence of optically thin disks. The last group of objects has  $[3.6] - [24] > 0.7$  and  $[3.6] - [24] > 0.4$  (i.e., they show excess at both IRAC and MIPS wavelengths). Most of these objects are likely to be optically thick disks. Figure 5b shows our sample of WTTSs combined with the sample of CTTTs. We note that the CTTTs populate exclusively the region of the diagram we associate with optically thick disks and that both WTTS and CTTT populations are very well mixed in this region of the diagram.

In Figure 6a we show the  $[3.6] - [4.5]$  versus  $[5.8] - [8.0]$  colors of WTTSs. In general, the populations of stars with and

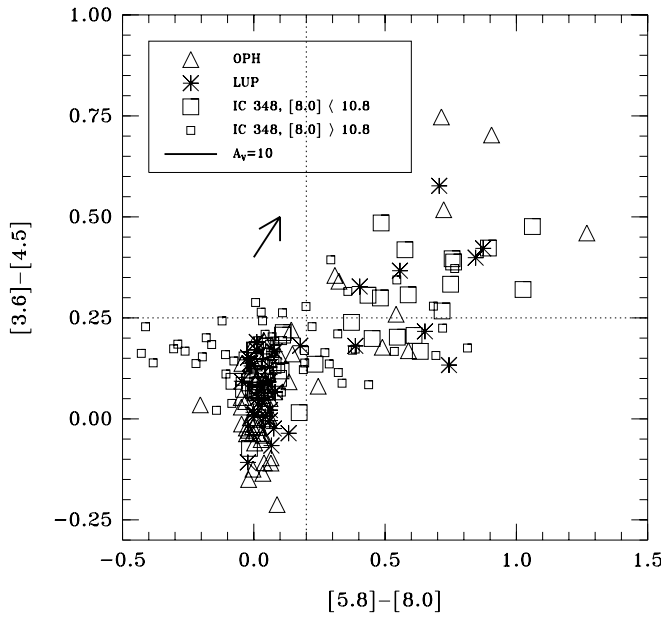


FIG. 6a

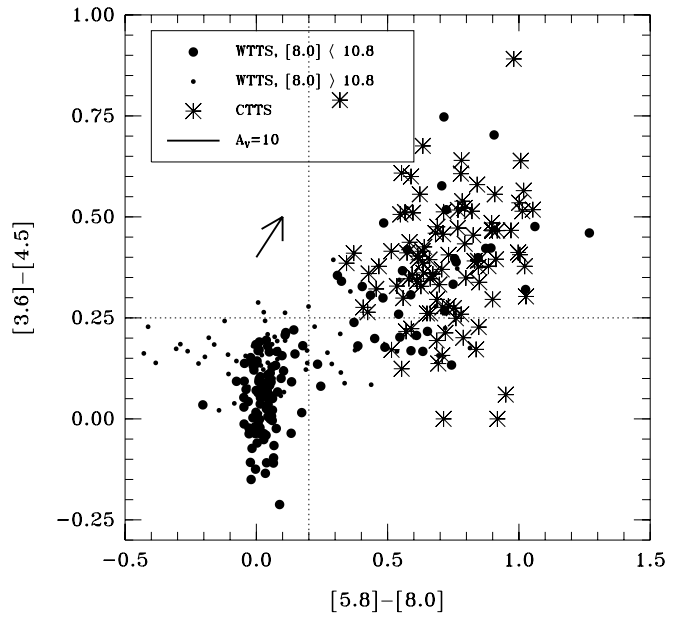


FIG. 6b

FIG. 6.—(a)  $[3.6] - [4.5]$  vs.  $[5.8] - [8.0]$  colors of our sample of WTTs. Faint IC 348 members ( $[8.0] > 10.8$  mag, 3 mJy) tend to have more uncertain colors than the rest of the sample and are shown as smaller open squares. The dotted lines represent the approximate boundaries of the color of the stellar photospheres. Asterisks in the upper right corner of the diagram have both 4.5 and 8.0  $\mu\text{m}$  excesses. Asterisks in the lower right corner of the diagram are stars with 8.0  $\mu\text{m}$  excess but no 4.5  $\mu\text{m}$  excess. (b) Combination of our sample of WTTs with CTTs from Hartmann et al. (2005) and L06.

without an excess are clearly separated. Stars in the upper right corner of the diagram have both 4.5 and 8.0  $\mu\text{m}$  excesses. Stars in the lower right corner of the diagram are stars with 8.0  $\mu\text{m}$  excess but no 4.5  $\mu\text{m}$  excess. These objects are usually interpreted as “transition disks” with inner holes (e.g., Calvet et al. 2002; D’Alessio et al. 2005). In fact, Sicilia-Aguilar et al. (2006) define transition disks as objects with 8.0  $\mu\text{m}$  excess but no 4.5  $\mu\text{m}$  excess. They find that only  $\sim 10\%$  of the T Tauri disks in the 4 Myr old cluster Tr 37 fall into this category. In contrast, we find that  $\sim 30\%$  of the WTTs are in fact transition disks according to the working definition stated above. This is in good agreement with the idea that WTTs disks represent a more evolved evolutionary state than CTTs disks. In Figure 6b we combine WTTs and CTTs in the same color-color diagram.

### 3.2.2. EW(H $\alpha$ ) Dependence?

Since the distinction between CTTs and WTTs is based on the H $\alpha$  EW, and CTTs show a much higher disk fraction than WTTs, we investigate the dependence of the IRAC disk fraction on H $\alpha$  EW within our sample of WTTs. We restrict our analysis to the 198 objects in the magnitude-limited subsample discussed in § 3.1.2. Figure 7a shows a histogram of the H $\alpha$  EW of stars with and without a disk, while Figure 7b shows the disk fraction versus H $\alpha$  EW. We find that (1) the disk fraction is highly correlated with H $\alpha$  and (2) the disk fraction is a smooth function of H $\alpha$  EW, increasing from  $\sim 5\%$  for the stars with H $\alpha$  observed in absorption to  $> 50\%$  for the stars with  $15 \text{ \AA} > \text{H}\alpha \text{ EW} > 10 \text{ \AA}$ .

Since a strong correlation between the presence of a disk and H $\alpha$  emission of chromospheric origin would be difficult to explain, the correlation observed in Figure 7 is likely to be driven by the presence of weakly accreting stars in our sample of WTTs. Multiepoch high-resolution spectroscopy of the sample of WTTs with disks would be highly desirable to establish, from their H $\alpha$  velocity profiles, which objects are in fact actively accreting (White & Basri 2003).

### 3.2.3. Disk Fraction Dependence on Spectral Type?

L06 find that the “optically thick” disk fraction in the entire populations of PMS stars (CTTs/WTTs) in IC 348 seems to be a function of spectral type. They argue that the disk fraction peaks around K6–M2 stars, which at the age of the cluster corresponds to stars with masses similar to that of the Sun, and conclude that circumstellar disks might last longer around solar type stars than around both less and more massive stars. Similarly, Carpenter et al. (2006) studied a sample of over 200 PMS stars in the 5 Myr old Upper Scorpius OB association with masses between  $\sim 0.1$  and  $20 M_{\odot}$  and found that stars with K–M spectral types have a significantly larger disk fraction than stars with G–B spectral types.

In order to investigate the possibility of a disk fraction dependence on spectral type for WTTs, we restrict our analysis to the 198 objects in the magnitude-limited subsample discussed in § 3.1.2 and divide our sample into the same three spectral type bins studied by L06. We find the following IRAC disk fractions for the three bins:  $28\% \pm 7\%$  (12/42) for stars with spectral types K6 and earlier,  $16\% \pm 5\%$  (10/62) for K7–M2 stars, and  $19\% \pm 4\%$  (18/94) for M2–M6 stars. Our result is inconsistent with a disk fraction of WTTs peaking around K6–M2 stars and suggests that the disk fraction dependence on spectral type found by L06, if real, is likely to be driven by the CTT population, which would imply that the duration of the *accretion phase* is a function of spectral type. Given the very different spectral type distribution of our sample (there are only seven objects with types later than K0 in our sample), our result does not contradict those presented by Carpenter et al. (2006).

### 3.2.4. Fractional Disk Luminosity

The ratio of the disk luminosity to the stellar luminosity,  $L_{\text{disk}}/L_{*}$ , is a measurement of the fraction of the star’s radiation that is intercepted and reemitted by the disk plus any accretion luminosity. This quantity is intimately related to the evolutionary status of a

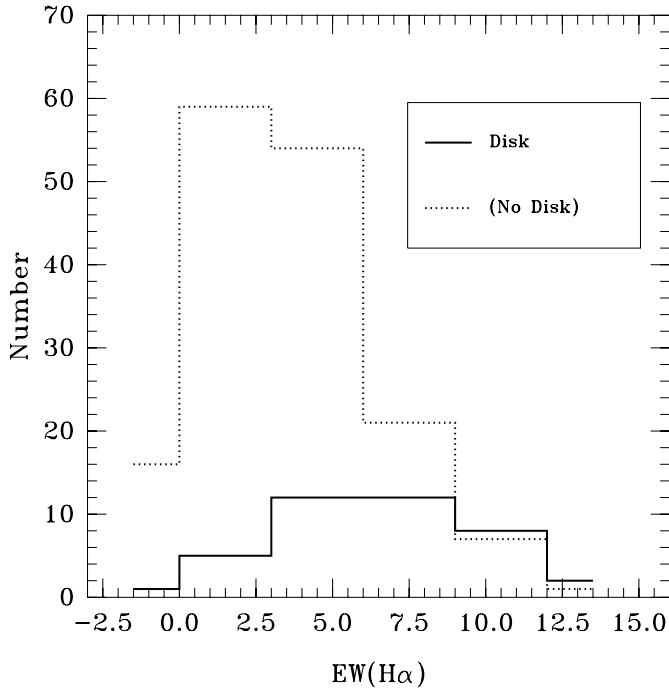


FIG. 7a

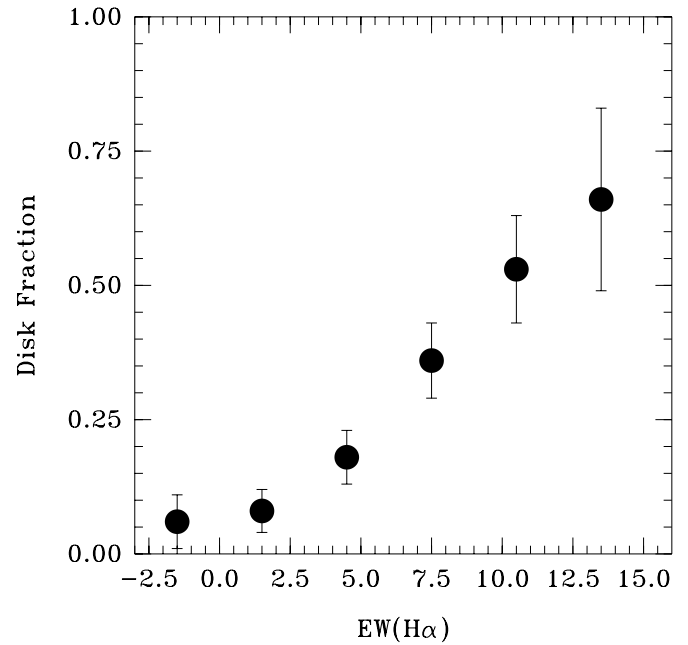


FIG. 7b

FIG. 7.—(a) Histogram of the H $\alpha$  EW for stars with and without a disk; (b) disk fraction of WTTs vs. H $\alpha$  EW. The disk fraction of WTTs seems to be a smooth function of H $\alpha$  EW.

circumstellar disk. On the one hand, the primordial, gas-rich disks around CTTs have typical  $L_{\text{disk}}/L_*$  values  $>10\%-20\%$ . On the other hand,  $L_{\text{disk}}/L_*$  values for optically thin, gas-poor debris disks around MS stars range from  $10^{-3}$  to  $10^{-6}$  (Beichman et al. 2005). In order to characterize  $L_{\text{disk}}/L_*$  for WTTs disks, we estimate this quantity for all the WTTs disks in our sample except for the few disks in IC 348 for which 24  $\mu\text{m}$  fluxes are not available. These objects are below our 24  $\mu\text{m}$  sensitivity limits, and the disk luminosities obtained from the IRAC excesses alone would be highly uncertain.

We estimate the disk luminosity according to the following procedure. We first calculate the IR excess at IRAC wavelengths and at 24  $\mu\text{m}$  by subtracting from the observed fluxes the expected photospheric contributions predicted by the stellar models shown in Figures 2, 3, and 4. Then, the IR excess at 24  $\mu\text{m}$  is extrapolated to longer wavelengths assuming the emission of a blackbody peaking at 24  $\mu\text{m}$  (i.e.,  $T = 121 \text{ K}$ ) and diluted by an emissivity proportional to  $\lambda^{-1}$ . Also, the IR emission of the shortest significant IRAC excess is extrapolated to shorter wavelengths assuming blackbody emission. The temperature of the adopted blackbodies ranges from 1400 to 500 K depending on the IRAC band from which the IR excess is extrapolated. Finally, we calculate the total disk luminosities by integrating the observed and extrapolated IR excesses over frequency. Similarly, the stellar luminosities are calculated by integrating the fluxes of the stellar models shown in Figures 2, 3, and 4 over frequency. The distribution of  $L_{\text{disk}}/L_*$  for our sample of WTTs is shown in Figure 8. The  $L_{\text{disk}}/L_*$  values calculated using the same procedure for a sample of CTTs (from Cieza et al. 2005) and debris disks (from Chen et al. 2005) are shown for comparison. The  $L_{\text{disk}}/L_*$  values we derive for our sample should be considered lower limits because our assumption that the flux density peaks at 24  $\mu\text{m}$  may underestimate the flux contribution of cool material in the outer disk. However, since none of our disks are detected at 70  $\mu\text{m}$ , we can constrain the flux contribution of the outer disks that may be missing in our disk lu-

minosity estimates. For each object, we approximate the outer disk as a diluted blackbody peaking at 70  $\mu\text{m}$  (i.e.,  $T = 41 \text{ K}$ ) with a flux density equal to 45 mJy, the estimated 3  $\sigma$  limits of the c2d observations at 70  $\mu\text{m}$  (Evans et al. 2005). For objects in Lupus and Ophiuchus, this approach constrains the luminosities of the outer disks to the  $10^{-5}L_*$  to  $10^{-4}L_*$  range. For objects in IC 348,

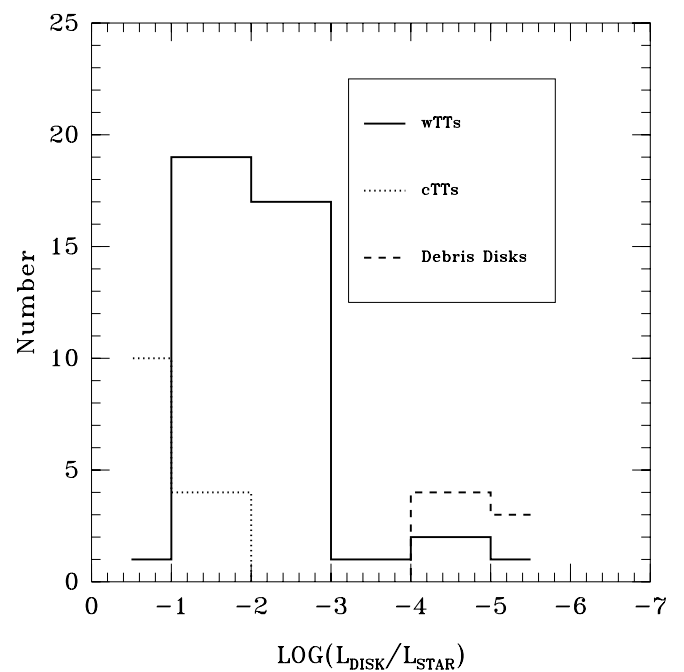


FIG. 8.—Fractional disk luminosities,  $L_{\text{disk}}/L_*$ , derived for our sample of WTTs disks. The  $L_{\text{disk}}/L_*$  values calculated using the same procedure for a sample of CTTs (from Cieza et al. 2005) and debris disks (from Chen et al. 2005) are shown for comparison. The  $L_{\text{disk}}/L_*$  values of WTTs disks fill the gap between the ranges observed for typical CTTs and debris disks, which are shown for comparison.

this range is  $10^{-3}L_*$  to  $10^{-4}L_*$ . Thus, we conclude that, for objects with warm disks for which we derive  $L_{\text{disk}}/L_* > 10^{-3}$ , the flux contribution of the outer disks is a small fraction of the total disk luminosity. For the objects for which we derive  $L_{\text{disk}}/L_* < 10^{-3}$ , the contribution of an unseen outer disk could, in principle, dominate the total disk luminosity. However, the disk luminosities of such cold disks would still remain in the debris disk range.

Figure 8 shows that only one object, Sz 96, has an  $L_{\text{disk}}/L_*$  value characteristic of CTTSs. This object is an M2 borderline CTTS/WTTS with an H $\alpha$  EW of 11 Å. As shown in Figure 2, the SED of Sz 96 shows strong IR excess at 2MASS wavelengths and is indistinguishable from that of a CTTS. This object is likely to be one of the actively accreting interlopers discussed in §§ 2.2 and 3.2.2. Similarly, only four objects have  $10^{-3} > L_{\text{disk}}/L_* > 10^{-6}$ , the range characteristic of optically thin debris disks. However, we note that the low luminosity and low optical depth of a disk do not necessarily warrant debris disk status, which requires the presence of a second generation of dust produced by the collision of planetesimals in a gas-poor environment. The lowest luminosity, and presumably optically thin, disks in our sample are RX J1622.6–2345, ROXs 36, IC 348-56, and IC 348-124. We model the SEDs of these disks in § 4.3. If these objects are in fact debris disks, at an age of  $\sim 1$ –3 Myr, they could be some of the youngest debris disks observed to date. However, the confirmation of debris disk status would require information on the grain size distribution and gas content of their disks. The main conclusion that can be drawn from Figure 8 is that the bulk of the WTTS disks have  $L_{\text{disk}}/L_*$  values that bridge the gap between the CTTSs and the debris disk range. This supports the idea that WTTS disks represent an intermediate evolutionary stage linking primordial disks around CTTSs and debris disks around MS stars.

## 4. DISCUSSION

### 4.1. Comparison to Recent Spitzer Results

#### 4.1.1. Comparison to P06

The IRAC disk fractions we found in § 3.1 are  $\sim 3$ –6 times larger than those recently found for a sample of 83 relatively isolated WTTSs (P06). P06 find that three of their objects show IR excess at both IRAC and MIPS wavelengths, while two objects show IRAC fluxes consistent with photospheric emission and small excesses at 24 μm. Most of these stars in the P06 sample are members of the extended population of Li-rich WTTSs discovered by the *ROSAT* X-ray satellite around nearby molecular clouds and are, for the most part, located outside the high-extinction regions mapped by the c2d project, but within  $\sim 6^\circ$  of the centers of the c2d cloud maps. The P06 observations were sensitive to the stellar photospheres of the entire sample at both IRAC wavelengths and 24 μm. Given the size of the samples involved, the discrepancy in the IRAC disk fraction of the off-cloud WTTSs studied by P06,  $4\% \pm 2\%$ , and that of the on-cloud WTTSs studied in this paper,  $20\% \pm 3\%$ , is significant at the  $4\sigma$  level.

Follow-up spectroscopic studies of *ROSAT* targets (e.g., Covino et al. 1997; Martin & Magazzu 1999; Wichmann et al. 2000) used the strength of the Li I λ6707 absorption line to discriminate bona fide PMS stars from young active MS stars (possibly  $\sim 100$  Myr old) sharing the same X-ray properties. P06 selected their sample from *ROSAT* WTTSs with Li I λ6707 absorption lines stronger than that of a Pleiades star of the same spectral type. These objects were suspected to be 1–10 Myr old because the age distribution of the *ROSAT* WTTSs, derived from their position in the H-R diagram, is not significantly different from that derived for the on-cloud T Tauri stars (Alcalá et al. 1997; see also § 4.4 of

this paper). This age estimate assumes that the *ROSAT* sources are located at the same distances as their adjacent molecular clouds. However, the distance and PMS status of the extended population of *ROSAT* sources have been called into question. Feigelson (1996) and Briceno et al. (1997) argue that the distributed population of *ROSAT* sources consists of mostly foreground post-T Tauri and active young ( $\sim 100$  Myr old) MS stars that are not necessarily associated with regions of current star formation (i.e., they are old enough to have moved far away from their birth sites) and that the presence of Li I λ6707 does not warrant PMS status since it is highly dependent on stellar mass, convection, and angular momentum history. The low disk fraction of the distributed population of *ROSAT* sources studied by P06 with respect to that of the sample of on-cloud WTTSs studied here supports the idea that the *ROSAT* sources found *around* molecular clouds represent a significantly older population of stars than that of the  $< 1$ –10 Myr old CTTSs and WTTSs found *within* molecular clouds. The age estimate of the extended population of Li-rich *ROSAT* sources depends on whether or not the P06/*ROSAT* targets are at the same distances as their adjacent molecular clouds. The luminosities of stars closer to us than the molecular clouds themselves could be considerably overestimated, translating into underestimated ages when the stars are placed in the H-R diagram. If the P06 sources are in fact associated with the molecular cloud and the sample has been biased toward foreground stars, the WTTSs in the P06 sample could be somewhat older than their nominal age of 1–10 Myr. It is reasonable to assume that such a bias toward foreground objects exists because P06 favored bright objects when selecting their sample in order to increase the number of WTTSs that could be observed at a given sensitivity. If the P06 sources are not associated with their adjacent molecular clouds, then the only age constraints are Li I λ6707 EW and X-ray brightness, and ages of the order of 100 Myr could not be ruled out.

#### 4.1.2. Comparison to L06

In a recent study of  $\sim 300$  confirmed members of IC 348 (WTTSs and CTTSs) L06 find an IRAC disk fraction of  $\sim 35\%$  among IC 348 members classified as WTTSs. The sample of WTTSs studied by L06 is virtually the same sample of IC 348 WTTSs included in this paper, for which we derive an IRAC disk fraction of  $23\% \pm 4\%$ . In what follows, we attempt to account for the difference in these results. L06 use a disk identification criterion based on the slope,  $\alpha$ , of a power-law fit to the four IRAC bands. From the comparison to disk models, they identify objects with  $\alpha > -1.8$  as optically thick disks. Based on the predicted slope of an M0 star and the typical uncertainty in the power-law fit, they identify objects with  $\alpha < -2.56$  as stellar photospheres and objects with intermediate slopes,  $-2.56 > \alpha > -1.8$ , as “anemic disks.” Cieza & Baliber (2006) suggest that many of the objects identified as anemic disks by L06 are more consistent with stellar photospheres of late M stars than with circumstellar disks. Based on a large sample ( $> 400$ ) of CTTSs and WTTSs from the literature with photometric uncertainties smaller than 0.1 mag, Cieza & Baliber (2006) find that CTTS and WTTS disks occupy a well-defined locus in the [3.6] – [8.0] versus [3.6] – [5.8] diagram with  $[3.6] - [8.0] > 0.7$ , while bare stellar photospheres have  $[3.6] - [8.0] < 0.5$ . In fact, only  $\sim 1\%$  of the objects in their sample have  $0.7 > [3.6] - [8.0] > 0.5$ . As seen in Figure 6, faint objects in IC 348, most of which are M4–M7 stars, have very uncertain [3.6] – [8.0] colors.

We suggest the possibility that the combined effect of slightly redder stellar photospheres and larger photometric uncertainties in late M stars with respect to brighter stars with earlier spectral types resulted in a large fraction of M4–M7 stellar photospheres

TABLE 4  
OBJECTS CLASSIFIED AS ANEMIC DISKS BY L06 THAT DO NOT SATISFY OUR DISK IDENTIFICATION CRITERION

R.A. (J2000.0)	Decl. (J2000.0)	ID (L06)	Spectral Type	$\alpha$ (L06)	$\sigma_\alpha$ (L06)	$(\alpha + 2.66)/\sigma_\alpha$ (L06)	[3.6] – [8.0] (L06)	[3.6] – [8.0] (c2d)	$\Delta([3.6] – [8.0])$ (L06–c2d)
55.9526.....	32.2308	261	M5	-2.560	0.048	2.0	0.29	0.26	0.03
55.9742.....	32.1251	254	M4.25	-2.549	0.081	1.3	0.30	0.29	0.01
56.0185.....	32.0817	303	M5.75	-2.197	0.125	3.7	0.61	...	...
56.0740.....	32.0799	169	M5.25	-2.440	0.099	2.2	0.41	0.36	0.05
56.0816.....	32.0403	322	M4.25	-2.426	0.046	5.0	...	...	...
56.0971.....	32.0318	1684	M5.75	-1.811	0.500	1.6	...	...	...
56.1203.....	32.0730	385	M5.75	-2.183	0.350	1.3	0.71	...	...
56.1309.....	32.1915	226	M5.25	-2.233	0.265	1.6	0.60	0.38	0.22
56.1358.....	32.1451	33	M2.5	-2.483	0.157	1.1	0.32	0.16	0.16
56.1365.....	32.1544	88	M3.25	-2.355	0.081	3.7	0.46	0.48	-0.02
56.1460.....	32.1269	8024	K7	-2.213	0.218	2.0	0.62	0.25	0.37
56.1590.....	32.1727	353	M6	-2.251	0.178	2.2	0.61	0.16	0.45
56.1794.....	32.1709	217	M5	-2.312	0.043	8.0	0.52	0.43	0.09
56.1822.....	32.1800	360	M4.75	-2.303	0.064	5.5	...	...	...
56.1861.....	32.1251	218	M5	-2.294	0.049	7.4	0.54	-0.04	0.58
56.1902.....	32.1864	413	M4	-2.398	0.500	0.5	...	0.31	...
56.2035.....	32.2228	178	M2.75	-2.520	0.080	1.7	0.31	0.23	0.08
56.2527.....	32.1387	344	M5	-2.376	0.229	1.2	0.49	0.45	0.04

being classified as anemic disks by L06. L06 find that the ratio of anemic disks to optically thick disks increases from  $\sim \frac{1}{5}$  to  $\sim 1$  from K6–M2 to M2–M6 stars, which is consistent with the idea that some of the anemic disks around late-type stars may be of questionable significance.

We find that most of the WTTSSs that do not satisfy our disk identification criterion discussed in § 3.1 but are classified as anemic disks by L06 are objects with spectral types M5 or later, which tend to have very uncertain IRAC colors due to the strong IR background of the IC 348 cluster. These low-mass objects account for the difference in the disk fraction derived by us and L06 for the WTTSSs in IC 348. In Table 4 we list the 18 objects classified as anemic disks by L06 that do not satisfy our disk identification criterion discussed in § 3.1. We find that, for objects in Table 4, the [3.6] – [8.0] colors obtained by L06 are  $\sim 0.15$  mag redder in the mean than our colors. However, this is a selection effect due to the fact that we are only considering the objects that have [3.6] – [8.0] colors from L06 that are red enough to be classified as anemic disks. In fact, when the entire sample of IC 348 WTTSSs is considered, our photometry gives [3.6] – [8.0] colors that are  $\sim 0.05$  mag *redder* than those obtained by L06. We note that even using the colors from L06, only one of the objects satisfies  $[3.6] – [8.0] > 0.7$ , the disk identification criterion proposed by Cieza & Baliber (2006). Also, for 12 of the 18 objects listed in Table 4, L06 derive  $\alpha$ -values that are consistent with the expected stellar photosphere within the errors [i.e.,  $(\alpha + 2.66)/\sigma_\alpha < 3$ , where  $-2.66$  is the slope of an M0 photosphere adopted by L06]. Finally, two of the objects for which  $(\alpha + 2.66)/\sigma_\alpha > 3$  have no 8.0  $\mu\text{m}$  fluxes measured by us or by L06, which renders the disk identification less reliable. We conclude that an accurate identification of weak IRAC excesses requires careful consideration of the photometric uncertainties involved, especially in regions with strong extended emission such as the IC 348 cluster.

#### 4.2. The Diversity and Evolutionary Status of WTTSS Disks

For late-type stars, the IRAC and MIPS fluxes originate from the inner  $\sim 20$  AU of the disk. For this reason, observations at these wavelengths are especially suited to study the evolution of the planet-forming region of the disk. According to models of

the evolution of circumstellar disks, dust growth and settling take place very efficiently in the circumstellar disks soon after their formation (Weidenschilling 1997; Dullemond & Dominik 2005). Numerical models also predict that the growth of dust will reduce the opacity of the disk to the stellar radiation, causing the disk to become flatter and the excesses in the mid-infrared to decrease with time proceeding from the shortest to the longest wavelengths. There is mounting evidence of such phenomena in the IRAC colors of T Tauri stars and lower mass objects (D'Alessio et al. 2001; Furlan et al. 2005; Sicilia-Aguilar et al. 2006; Muzerolle et al. 2006).

In this section we try to explore observational consequences that could be related to dust grain growth and/or settling toward the midplane for the sample of WTTSSs with disks. To this end, we estimate the longest wavelength *without* significant infrared excess from the dereddened SEDs,  $\lambda_{\text{turnoff}}$  (in  $\mu\text{m}$ ), and the slope of the SED longward of  $\lambda_{\text{turnoff}}$ ,  $\alpha_{\text{excess}}$ , for all the WTTSSs with disks in the sample. We compare these values for our sample of WTTSSs to those we obtain for a sample of CTTSs in Chamaeleon from Cieza et al. (2005) and a sample of debris disks from Chen et al. (2005). Figure 9 shows the ranges of mid-IR slopes  $\alpha_{\text{excess}}$  versus the wavelength of disk emission turnoff  $\lambda_{\text{turnoff}}$ . Systems with  $\lambda_{\text{turnoff}} \leq 2.0 \mu\text{m}$  show some excess in the near-IR JHK bands and are probably actively accreting (see, e.g., Hartmann et al. 2005; Muzerolle et al. 2003). Objects with  $\lambda_{\text{turnoff}}$  in the IRAC range are likely to be purely irradiated disks with increasing degree of settling and/or larger inner holes with increasing  $\lambda_{\text{turnoff}}$ . Finally, those stars with  $\lambda_{\text{turnoff}} \geq 8.0 \mu\text{m}$  are likely to have cleared inner disks with radii of several AU (e.g., Calvet et al. 2002) or alternatively have dust in the inner disk that has grown to sizes large enough not to produce any detectable excess above the photospheric level.

A simple disk evolution scenario based solely on dust grain growth and settling predicts smaller  $\alpha_{\text{excess}}$  slopes for longer  $\lambda_{\text{turnoff}}$  or larger cleared inner regions (Dullemond & Dominik 2005; D'Alessio et al. 2005). However, Figure 9 suggests that the *range of possible excess slopes increases with the process of inner disk clearing*. The actively accreting CTTSs all cluster around  $\alpha_{\text{excess}}$  values of  $-1$ . For these objects, the onset of the IR excess occurs near 2.2  $\mu\text{m}$ . We find that WTTSSs show a richer

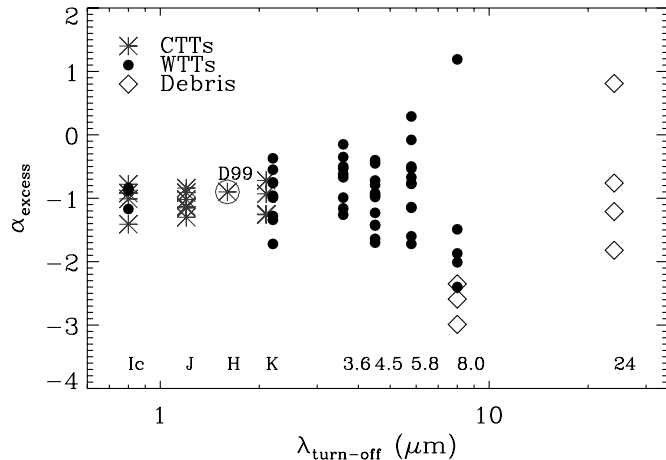


FIG. 9.—Distribution of excess slopes  $\alpha_{\text{excess}}$  vs. the wavelength at which the infrared excess begins  $\lambda_{\text{turnoff}}$  for the sample of WTTs (filled circles), a sample of CTTs in Chamaeleon from Cieza et al. (2005), the median SED of CTTs in Taurus from D'Alessio et al. (1999) in asterisks (marked as D99), and a sample of debris disks from Chen et al. (2005) in diamonds. The diagram shows a much larger spread in inner disk morphologies of WTTs with respect of those of CTTs. [See the electronic edition of the Journal for a color version of this figure.]

distribution of SED morphologies than CTTs. Some of the WTTs show SEDs that are indistinguishable from those of CTTs, while others show a wide range of  $\lambda_{\text{turnoff}}$  and  $\alpha_{\text{excess}}$  values. Finally, the debris disks, with ages 12 and 200 Myr (Chen et al. 2005), show detectable excess only longward of  $8.0 \mu\text{m}$ , but they also present a great variety of spectral slopes.

In general, the diagram suggests an evolutionary sequence in which most actively accreting CTTs have similar near- to mid-IR SEDs, dominated by optically thick emission of the inner disk. This similarity is probably due to the fact that, in most cases, their inner disks extend to the dust sublimation radius (Muzerolle et al. 2003). On the other hand, if disks evolve from the inside out, WTTs disks are likely to have a wider range of inner disk radii and temperatures than CTTs. This diversity of inner disks, together with possible grain growth and grain settling to the disk midplane, may explain the large ranges of  $\alpha_{\text{excess}}$  and  $\lambda_{\text{turnoff}}$  found. Finally, the debris disks populate the right part of the plot with large cleared inner disks and emission from cool optically thin dust.

#### 4.3. Comparison to Optically Thin Disk Models

As discussed in § 3.2, four stars in our sample show SEDs and  $L_{\text{disk}}/L_*$  consistent with optically thin disks. These are ROXs 36, RX J1622.6–2345, IC 348-56, and IC 348-124. In this section we model these four objects using the optically thin disk model developed by Augereau et al. (1999).

We limited the exploration of the parameter space to the disk parameters that affect most the global shape of an SED, namely, the minimum grain size  $a_{\min}$ , the peak surface density position  $r_0$ , and the total dust mass  $M_{\text{dust}}$  (or, equivalently, the surface density at  $r_0$ ). We adopted a differential grain size distribution proportional to  $a^{-3.5}$  between  $a_{\min}$  and  $a_{\max}$ , with  $a_{\max} = 1300 \mu\text{m}$ , a value sufficiently large to not affect the SED fitting in the wavelength range we consider. Following Augereau et al. (1999), the disk surface density  $\Sigma(r)$  is parameterized by a two power-law radial profile  $\Sigma(r) = \Sigma(r_0)\sqrt{2(x^{-2\alpha_{\text{in}}} + x^{-2\alpha_{\text{out}}})^{-1/2}}$ , with  $x = r/r_0$ , and where  $\alpha_{\text{in}} = 10$  and  $\alpha_{\text{out}} = -3$  to simulate a disk peaked around  $r_0$ , with a sharp inner edge, and a density profile decreasing smoothly with the distance from the star beyond  $r_0$ . The optical properties of the grains were calculated for astronomical silicates (optical constants from Weingartner & Draine 2001) and with the Mie theory valid for hard spheres. The grain temperatures were obtained by assuming that the dust particles are in thermal equilibrium with the central star. NextGen model atmosphere spectra (Hauschildt et al. 1999) scaled to the observed dereddened K-band magnitude were used to model the stellar photospheres.

For each star, we calculated 15,000 SEDs ( $0.3 \mu\text{m} \leq \lambda \leq 950 \mu\text{m}$ ) for 75 logarithmically spaced values of  $a_{\min}$  between 0.05 and  $100 \mu\text{m}$  and for 200 values of  $r_0$ , logarithmically spaced between 0.02 and 300 AU. For each model, the dust mass was adjusted by a least-squares method, assuming purely photospheric emission (within the uncertainties, 10%) in the four IRAC bands, and by fitting the measured MIPS 24  $\mu\text{m}$  flux density. Models with flux densities in the MIPS 70 and 160  $\mu\text{m}$  bands, larger than the estimated  $2\sigma$  upper limits of 0.03 and 0.5 Jy, respectively, were eliminated. The results are summarized in Table 5, and the SEDs are displayed in Figure 10. Results in Table 5 are listed for two different regimes of minimal grain sizes, namely,  $a_{\min} > 10 \mu\text{m}$  and  $a_{\min} < 0.5 \mu\text{m}$ . The first regime accounts for a scenario where all grains have grown to sizes  $> 10 \mu\text{m}$  and where smaller grains are not replenished by collisions, while the second regime accounts for a case where grains smaller than  $0.5 \mu\text{m}$  remain in the system, either because they are collisionally replenished or because pressure forces are inefficient to expel grains. However, assuming a gas-poor environment (i.e., the dust dynamics is not controlled by the gas), dissipation processes acting on small grains will limit the size of the smallest grains that are likely to populate the disk. For ROXs 36, an A2 star, the blowout size is of the order of a few microns. Thus, grains significantly smaller than  $0.5 \mu\text{m}$  are unbound and unlikely to be present in the disk. For the three M-type stars, radiation pressure is not high enough to overcome the gravitational force and expel grains. In this case, and provided that the star mass-loss rate is high enough, the pressure force expected from the stellar wind will set the lower limit for  $a_{\min}$  (Augereau & Beust 2006; Strubbe & Chiang 2006).

In most cases, neither the position of the peak surface density  $r_0$  nor the minimum grain size  $a_{\min}$  can be uniquely determined

TABLE 5  
OPTICALLY THIN DISK PROPERTIES, FOR TWO DIFFERENT REGIMES OF MINIMAL GRAIN SIZES,  $a_{\min}$

STAR	$a_{\min} < 0.5 \mu\text{m}$			$a_{\min} > 10 \mu\text{m}$			
	$r_0$ (AU)	$M_{\text{dust}}$ ( $10^{-3} M_{\oplus}$ )	$t_{\text{coll}}$ (yr)	$r_0$ (AU)	$M_{\text{dust}}$ ( $10^{-3} M_{\oplus}$ )	$t_{\text{coll}}$ (yr)	$L_{\text{IR}}/L_*$ ( $\times 10^3$ )
ROXs 36 .....	$82^{+100}_{-73}$	$6.7^{+25}_{-6.5}$	$77000^{+10000}_{-74000}$	$17^{+2.8}_{-10}$	$5.3^{+5.9}_{-4.9}$	$7400^{+1900}_{-5200}$	$0.11^{+0.015}_{-0.023}$
RX J1622.6–2345 .....	$4.0^{+51}_{-51}$	$0.13^{+280}_{-0.13}$	$310^{+2000}_{-300}$	$1.9^{+6.1}_{-1.4}$	$0.35^{+85}_{-0.34}$	$130^{+79}_{-110}$	$0.60^{+5.4}_{-0.11}$
IC 348-56 .....	$5.2^{+59}_{-4.4}$	$0.53^{+570}_{-0.52}$	$190^{+1300}_{-190}$	$2.5^{+6.7}_{-1.8}$	$1.5^{+180}_{-1.5}$	$86^{+32}_{-70}$	$1.4^{+9.7}_{-0.27}$
IC 348-124 .....	$4.1^{+27}_{-3.2}$	$0.74^{+170}_{-0.69}$	$65^{+330}_{-61}$	$1.8^{+2.4}_{-0.94}$	$1.8^{+33}_{-1.6}$	$24^{+15}_{-14}$	$3.1^{+8.6}_{-0.65}$

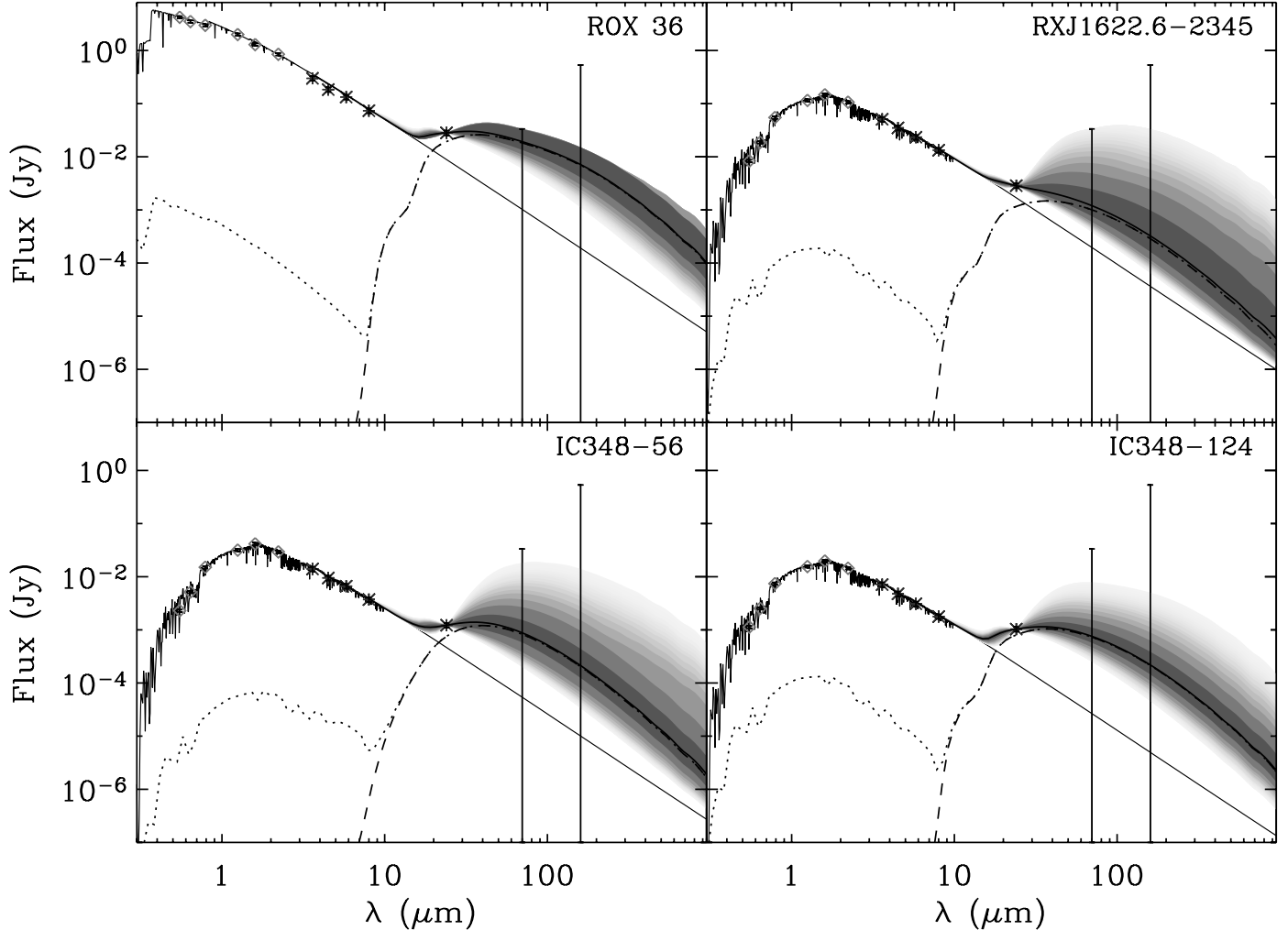


FIG. 10.—WTTSSs with  $24\text{ }\mu\text{m}$  excess consistent with optically thin disks. On each plot, the darkest regions correspond to the most likely fits to the SEDs. The dashed line shows the thermal emission for the best-fit model, while the dotted line corresponds to the total disk emission (i.e., including scattered light emission).

with so few observational constraints, but some models can be eliminated. In particular, the lack of excess in the IRAC bands imposes the disk to be significantly dust depleted within  $\sim 1$  AU from the star. The best fits to the SEDs of the three low-mass stars (RX J1622.6–2345, IC 348-56, and IC 348-124) are indeed obtained for  $r_0$  values around 2–5 AU, while in the case of ROXs 36, the inner hole could be 10 times larger. The properties of the ROXs 36 disk are in fact those of a typical  $\beta$  Pic-like disk: a dust mass in the  $10^{-4}$  to  $10^{-2} M_{\oplus}$  range, a low fractional luminosity  $L_{\text{IR}}/L_{*}$  of about  $10^{-4}$ , and typical minimum collision timescales (as calculated using the formula given by Backman & Paresce 1993) 1–3 orders of magnitude smaller than the star age. Also, as it is the case for virtually all  $\beta$  Pic-like disks, the disk around ROXs 36 seems to be collisionally dominated because collisions occur much faster than Poynting-Robertson (P-R) drag (as calculated using the formula given by Augereau & Beust 2006) for all grains larger than the blowup size. The best fits to the observed excesses around the three low-mass WTTSSs (RX J1622.6–2345, IC 348-56, and IC 348-124) are also consistent with optically thin disks observed around other young M-type stars such as AU Mic (Liu et al. 2004). These three objects have low luminosity ratios,  $L_{\text{IR}}/L_{*} < 2 \times 10^{-2}$ , and dust masses between  $10^{-4}$  and  $10^{-3} M_{\oplus}$ , with an upper limit of about  $0.5 M_{\oplus}$ . The collision timescales for these three objects are extremely small (of the order of 100 yr).

The preliminary models described above suggest that the disks around ROXs 36, RX J1622.6–2345, IC 348-56, and IC 348-124 could be younger analogs of the  $\beta$  Pic and AU Mic debris disks, and thus some of the youngest debris disks ever observed. However, this interpretation depends on the assumption that these four WTTSS disks are gas-poor (as their older counterparts are). The timescale over which gas clearing occurs is still poorly constrained observationally, and it is even unclear whether gas and dust are lost simultaneously as disks evolve from the massive optically thick to the debris disk phase. High-resolution *Spitzer* IRS observations, such as those presented by Pascucci et al. (2006), to constrain the amount of gas present in these extremely young (1–3 Myr) optically thin disks could provide crucial information on the gas evolution in the transition from the primordial to the debris disk stage.

In § 3.1 we found that most WTTSSs ( $\sim 80\%$ ) show no evidence for a disk. Since *Spitzer* observations are capable of detecting very small amounts of dust in the planet-forming regions of the disk ( $r \sim 0.1$ –10 AU), the absence of mid-IR excess imposes very stringent limits on the amount of dust available for planet formation around “diskless” WTTSSs (i.e., most WTTSSs). In this section we use the optically thin disk models discussed above to constrain the maximum amount of dust that could remain undetected within the first few tens of AU of the WTTSSs in our sample. Since the

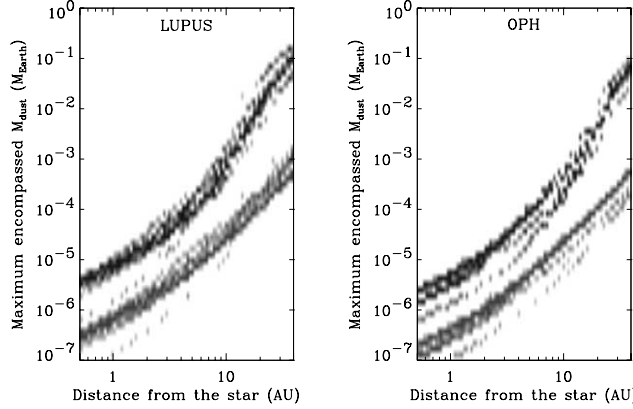


FIG. 11.—Maximum encompassed dust mass as a function of the distance from the star for the Lupus (left) and Ophiuchus (right) clouds. The bottom area corresponds to mass upper limits when minimum grain sizes  $a_{\min}$  between 0.05 and 0.5  $\mu\text{m}$  are considered, while the top area corresponds to 10  $\mu\text{m} < a_{\min} < 100 \mu\text{m}$ . [See the electronic edition of the Journal for a color version of this figure.]

24  $\mu\text{m}$  observations are the most constraining, we restrict our analysis to Lupus and Ophiuchus objects that have 24  $\mu\text{m}$  fluxes consistent with stellar photospheres and exclude the objects that remain undetected at this wavelength. Objects in IC 348 are also excluded because we detect the stellar photospheres of only a couple of them.

Since none of our “diskless” WTTSSs are detected in the c2d 70 and 160  $\mu\text{m}$  maps, for the purpose of our models, we adopt nominal upper limits of 15 and 250 mJy at 70 and 160  $\mu\text{m}$ , respectively. For each model we calculated the mass encompassed within a radius  $r$ , as a function of this radius. With this approach, we can estimate the maximum dust mass in the inner regions of the WTTSSs with no detectable, or marginally detected, emission in excess to the photospheric emission. The results are displayed in Figure 11 for the Lupus and Ophiuchus clouds, assuming distances to the Sun listed in Table 6. For the Lupus and Ophiuchus clouds, the c2d *Spitzer* observations constrain the observed WTTSSs to have less than a few times  $10^{-6} M_{\oplus}$  of dust within 1 AU from the central star, and less than a few times  $10^{-4} M_{\oplus}$  within 10 AU. These mass upper limits, obtained for minimum grain sizes between 10 and 100  $\mu\text{m}$ , drop by about an order of magnitude when  $a_{\min} \leq 0.5 \mu\text{m}$ . The Lupus and Ophiuchus WTTSSs with no (or marginal) excess at 24  $\mu\text{m}$  have then inner disks that are strongly depleted, and only extremely cold disks with large inner holes are still theoretically possible because of the relatively large MIPS 70 and 160  $\mu\text{m}$  upper limits. Such belts would resemble the dust rings resolved about nearby young MS stars (e.g., HD 181327; Schneider et al. 2006 and references therein). Of course, our observations only constrain the mass of dust and cannot rule out the presence of much larger planetesimals or planets because once dust grains grow into larger bodies ( $r \gg \lambda$ ), most of the solid mass never interacts with the radiation, and the opacity function,  $k_{\nu}$  ( $\text{cm}^2 \text{g}^{-1}$ ), decreases dramatically.

#### 4.4. Circumstellar Disks and Stellar Ages

In § 3.1 we studied the overall disk fraction of our sample of WTTSSs. In this section we derive stellar ages from two different evolutionary tracks and estimate the disk frequency as a function of stellar age. In order to derive stellar ages from theoretical evolutionary tracks, it is necessary to obtain the effective temperatures and luminosities of all the targets. We estimate the effective temperatures directly from the spectral type of the objects according to the scale provided by Kenyon & Hartmann (1995). We derive the

TABLE 6  
ADOPTED DISTANCES

Cloud	Distance (pc)	References
Ophiuchus .....	125 $\pm$ 20	de Geus et al. (1989)
Lupus I .....	150 $\pm$ 20	F. Comeron et al. (2007, in preparation)
Lupus III .....	200 $\pm$ 20	F. Comeron et al. (2007, in preparation)
IC 348 .....	320 $\pm$ 30	Herbig (1998)

stellar luminosities by applying a bolometric correction (appropriate for each spectral type) to the 2MASS  $J$ -band magnitudes corrected for extinction and assuming the nominal cloud distance listed in Table 6. The  $J$  band was chosen because the effects of extinction are less important than at shorter wavelengths ( $A_J \sim 0.26 A_V$ ) and the emission from the disk is less prominent than at longer wavelengths. The bolometric corrections were taken from Hartigan et al. (1994), and the  $J$ -band extinction,  $A_J$ , was calculated using  $A_J = 1.24E(R_C - I_C) = 1.24[(R_C - I_C)_{\text{obs}} - (R_C - I_C)_0]$ . The intrinsic stellar colors,  $(R_C - I_C)_0$ , come from Kenyon & Hartmann (1995). For objects without  $R_C$  and  $I_C$  fluxes available, we use  $A_J = 5.88E(J - K)$ .

#### 4.4.1. Estimation of Age Uncertainties

In order to estimate the error bars associated with the ages we derive, we first estimate the observational uncertainties that need to be propagated through the H-R diagram. Fortunately, the  $T_{\text{eff}}$  values and luminosities of WTTSSs are easier to determine than those of CTTSSs. The interplay between extinction and veiling introduces a large uncertainty in determining stellar luminosities of CTTSSs, and different results are obtained depending on the band to which the bolometric correction is applied (Cieza et al. 2005). In fact, the luminosities obtained from the  $J$  band are systematically larger (by  $\sim 35\%$ ) than those obtained from the  $I_C$  band. For WTTSSs, Cieza et al. (2005) show that the luminosities derived from the  $I_C$  and  $J$  bands agree to within 5%; therefore, distance is probably the dominant uncertainty in calculating their luminosity. The distance uncertainties listed in Table 6 translate into  $\sim 20\%-30\%$  luminosity uncertainties. Similarly, the spectral type classification of WTTSSs (and therefore their temperatures) is usually more accurate than that of CTTSSs. This is because the spectra of CTTSSs are affected by veiling, and their photospheres are highly heterogeneous in terms of temperature due to the presence of hot accretion columns. To estimate the effective temperature uncertainty of the WTTSSs in our sample, we adopt one spectral type subclass as the classification accuracy. For the reasons mentioned above, we regard the  $T_{\text{eff}}$  values and the luminosities (and therefore the ages) of WTTSSs as being more accurate than those derived for CTTSSs using the same procedure.

A study of the disk fraction as a function of age can only yield meaningful results if the intrinsic age spread of the sample is larger than the age uncertainties attributable to observational errors. We verify that our sample satisfies this condition by comparing the spread of the ages we derive to that expected solely from observational errors. Based on an error budget similar to the one described above, Hartman (2001) estimated that observational errors will introduce an age spread of  $\sigma \log(\text{age}) = 0.18$  in the logarithmic age distribution derived for WTTSSs in Taurus. In Figure 12 we plot the derived age distribution of our sample as calculated from two different evolutionary tracks. The mean age and the age spread are model dependent. According to the models presented by D’Antona & Mazzitelli (1994) and D’Antona &

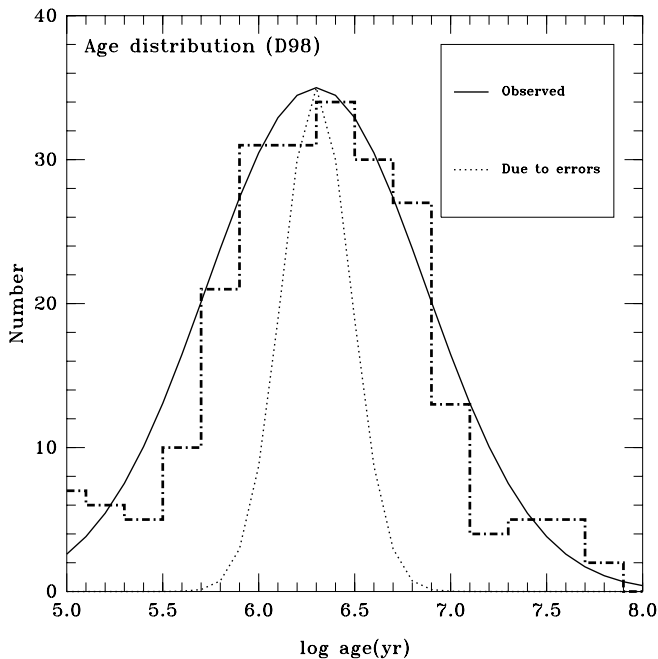


FIG. 12a

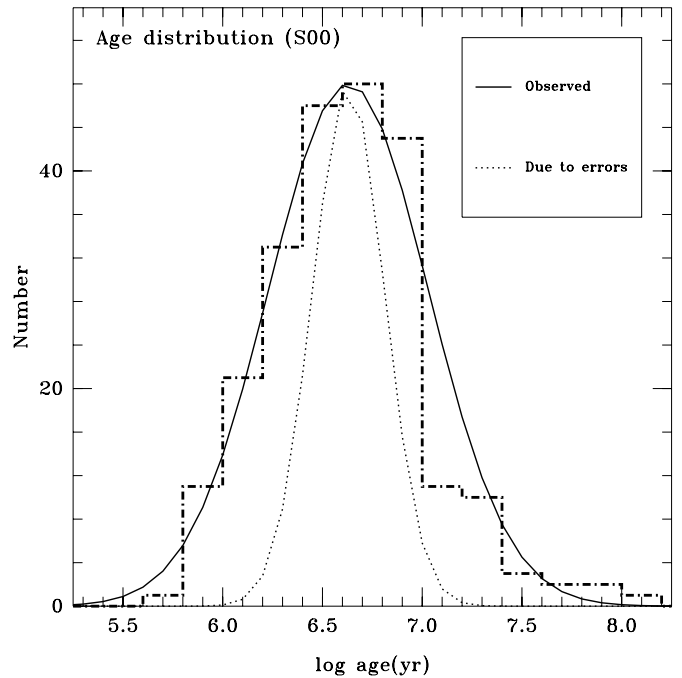


FIG. 12b

FIG. 12.—Distributions of stellar ages obtained for our sample using the (a) DM98 and (b) S00 evolutionary tracks. The observed age distributions (solid lines) are significantly wider than what is expected from the propagation of observational errors into derived stellar ages (dotted lines).

Mazzitelli (1998, hereafter DM98),<sup>14</sup> the logarithmic age distribution of our sample can be characterized as a Gaussian centered around  $\log(\text{age}) = 6.3$  with  $\sigma \log(\text{age}) = 0.57$ . Similarly, according to the models presented by Siess et al. (2000, hereafter S00),<sup>15</sup> the logarithmic age distribution of the sample can be characterized as a Gaussian centered around  $\log(\text{age}) = 6.6$  with  $\sigma \log(\text{age}) = 0.40$ . The age spreads derived are 2.2–3.2 times the value attributed by Hartmann (2001) to observational errors, which is also shown in Figure 13 for comparison.

#### 4.4.2. Evolutionary Tracks and Stellar Ages

In order to evaluate the degree to which ages we derive depend on the models, we compare the individual ages derived from the DM98 and S00 models. We choose these two particular evolutionary tracks because they provide the appropriate mass and age range and are both widely used, which allows a direct comparison of our results to those from other papers. Figure 13a shows the ages derived for our sample using both sets of evolutionary tracks. The error bars for every object have been calculated by propagating into the evolutionary tracks the *observational* uncertainties computed as described in the previous section (e.g., a  $T_{\text{eff}}$  uncertainty equal to one spectral type subclass and a luminosity uncertainty dominated by the distance uncertainty). Stellar ages of PMS stars are very difficult to estimate due to the large observational and model uncertainties involved (Hillenbrand & White 2004), and they are often taken with a high degree of (healthy) skepticism. However, even though the error bars in the individual ages are large, the total age spread in the sample is significantly larger than the typical (observational) error bar. This is consistent with the analysis of Figure 12. Also, even though DM98 and S00 evolutionary tracks show some systematic differences (e.g., DM98 tracks yield significantly younger ages than S00 models), the relative ages agree fairly well.

Figure 13a shows that ~40% of the WTTSSs that are both younger than 1.5 Myr according to the S00 models *and* younger than 0.6 Myr according to the DM98 models have circumstellar disks. In contrast, none of the targets that are older than 10 Myr according to the DM98 or S00 models has a disk. The decrease in the IRAC disk fraction with stellar age is clearly seen Figure 13b, where we restrict our analysis to the 198 objects in the magnitude-limited subsample discussed in § 3.1.2 and divide the ages we derive using the DM98 and S00 models into four age bins. Very similar conclusions can be drawn if our sample is combined with that of P06. Including the P06 samples considerably increases the statistical significance of the last age bin. Taking both samples together, none of the ~40 stars that are older than 10 Myr according to either of the tracks have an IR excess indicating the presence of a circumstellar disk.

#### 4.5. Constraint on the Timescale of Planet Building

Figure 13 suggests that circumstellar disks, as defined by the presence of IR excesses at  $\lambda \leq 10\text{--}24 \mu\text{m}$ , are very rare or non-existent around WTTSSs with ages  $\gtrsim 10$  Myr. This timescale is very similar to that obtained by studies of the frequency of circumstellar disks detected in the near-IR (for a review see Hillenbrand 2006). However, our results impose much stronger constraints on the time available for the formation of planets than those provided by previous studies. Past results based on near-IR excesses always left room for the possibility that stars without near-IR excess had enough material to form planets at larger radii not probed by near-IR wavelengths. *IRAS* and *ISO* had the appropriate wavelength range to probe the planet-forming regions of the disk but lacked the sensitivity needed to detect all but the strongest mid- and far-IR excesses in low-mass stars at the distances of nearest star-forming regions. *Spitzer* provides, for the first time, the wavelength coverage and the sensitivity needed to detect small amounts of dust in the planet-forming regions of a statistically significant number of low-mass PMS stars. In particular, the results from § 4.3 suggest that

<sup>14</sup> Available at <http://www.mporzio.astro.it/~danton/prehms.html>.

<sup>15</sup> Available at <http://www-astro.ulb.ac.be/~siess/database.html>.

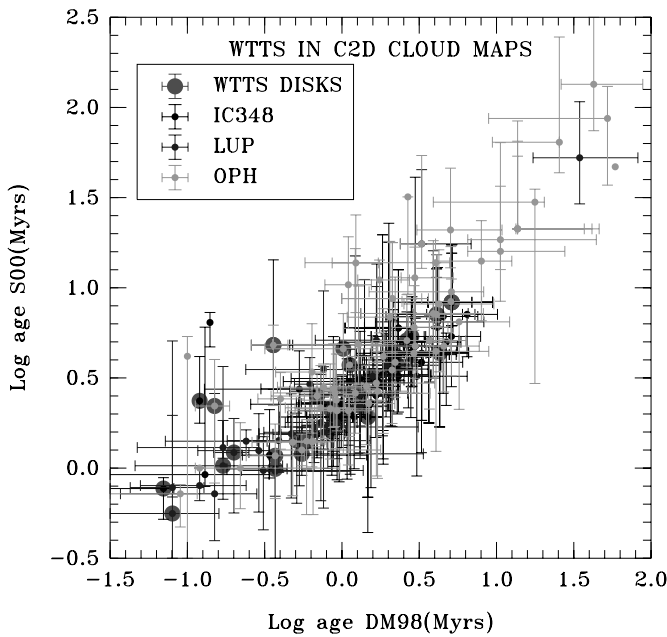


FIG. 13a

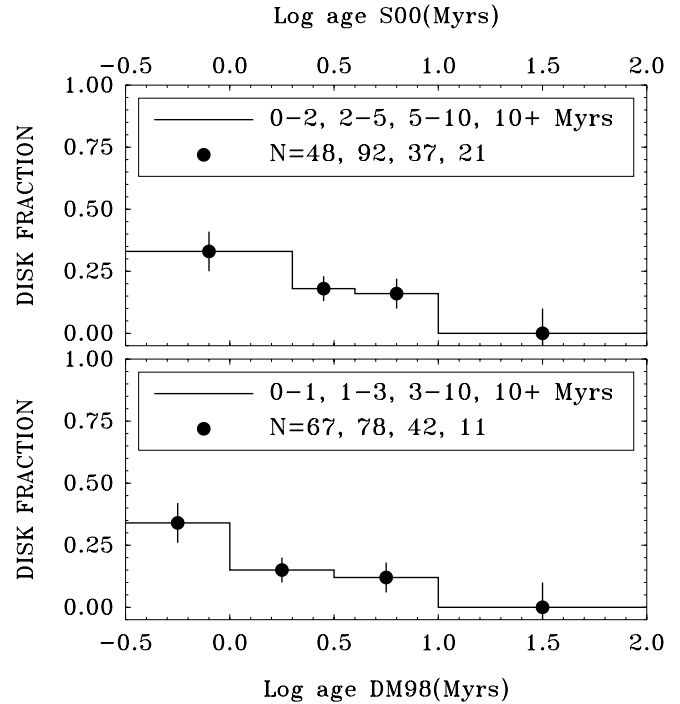


FIG. 13b

FIG. 13.—Stellar ages derived for our sample of WTTTs using two different sets of evolutionary tracks (DM98 and S00). The error bars have been calculated adopting a  $T_{\text{eff}}$  uncertainty equal to one spectral type subclass and a luminosity error calculated from the uncertainty in the distance (*a*). A clear decrease in the disk fraction is seen with increasing age. Roughly 40% of the targets that are both younger than 1 Myr according to DM98 tracks and younger than 2 Myr according to S00 tracks have disks. None of the stars that are older than  $\sim 10$  Myr according to either of the models have disks (*b*). [See the electronic edition of the Journal for a color version of panel (*a*) of this figure.]

$24 \mu\text{m}$  fluxes consistent with stellar photospheres constrain the amount of *warm* dust ( $T \sim 100$  K) in the disks of our sample of WTTTs to be much less than an Earth mass. Even though our  $24 \mu\text{m}$  observations are not sensitive to the stellar photospheres of all the targets, taking the P06 sample and our sample together, there are at least  $\sim 40$  WTTTs with estimated ages  $> 10$  Myr showing photospheric fluxes at  $24 \mu\text{m}$ . This number is likely to be a lower limit because, as discussed in § 4.1.2, we suspect that the ages of many of the stars in the P06 sample have been underestimated. This seems to imply that after  $\sim 10$  Myr WTTTs have to be in a relatively advanced stage of the planet formation process if they are to form planets at all.

Since the CTTS disks older than 10 Myr are also very infrequent, 10 Myr seems to be a general upper limit for the survival of primordial disks around PMS stars. This conclusion is also supported by recent results from the “Formation and Evolution of Planetary Systems” (FEPS) project. Silverstone et al. (2006) search for IRAC excesses in a sample of 74 young (age  $< 30$  Myr old) Sun-like ( $0.7 < M_*/M_{\odot} < 1.0$ ) stars. They divided the sample into two age bins, 3–10 Myr and 10–30 Myr. Silverstone et al. (2006) find IRAC excesses for 4 of the 29 stars in the youngest age bin and for 1 of the 45 stars in the older age bin. The FEPS objects were selected based on their ages ( $< 30$  Myr), masses ( $\sim 1 M_{\odot}$ ), distances ( $< 170$  pc), and low infrared backgrounds, without a bias with respect to their H $\alpha$  EW or IR properties. The five objects with IRAC excess have SEDs consistent with those of CTTSs, and given the age uncertainties, it is entirely possible that they are all younger than 10 Myr. In fact, the only object with IRAC excess for which Silverstone et al. (2006) adopt an age older than 10 Myr is PDS 66. Silverstone et al. (2006) adopted an age of 17 Myr for PDS 66 based on the mean age of the Lower Centaurus Crux, but its formal age is 7–17 Myr depending on the evolutionary track used (Mamajek et al. 2002). Recent submillimeter results extend

the conclusions on the survival time of the material in the inner disk ( $r < 0.1$  AU) and the planet-forming region of the disk ( $r \sim 1$ –10 AU) to the outer disk ( $r \sim 100$  AU). Andrews & Williams (2005) observed over 150 YSOs in Taurus and found that  $< 10\%$  of the objects lacking inner disk signatures were detected at submillimeter wavelengths. Given the high sensitivity of their survey ( $3\sigma \sim 10$  mJy at  $850 \mu\text{m}$ ), they conclude that dust in the inner and outer disks dissipates nearly simultaneously.

Figure 13 also suggests that the disks of some WTTTs dissipate in timescales  $\lesssim 1$  Myr.<sup>16</sup> Are these apparently very young diskless objects as young as the evolutionary tracks suggest, or is their apparent youth just a product of the large age uncertainty? Several factors can introduce very large errors in the age determination. For instance, the luminosity of foreground field stars can be grossly overestimated if the nominal cloud distances are used, leading to grossly underestimated ages. Also, large errors in the spectral type classification might lead to large errors in the extinction and luminosities. To check for these possibilities, we plotted the SEDs of the objects classified as the youngest diskless WTTTs in our sample. Their SEDs look consistent with stellar photospheres, and the overall quality of the fits suggests that both the spectral types and the extinction corrections are reasonably accurate. Still, some of these objects are  $\sim 0.5$  Myr old according to the DM98 models and  $\sim 1.0$  Myr old according to the S00 models, as well as  $\sim 15$  times more luminous than MS stars of the corresponding spectral types.

In § 4.4 we found that the dissipation timescale or “survival time” of WTTs circumstellar disks ranges from less than 1 to

<sup>16</sup> This assumes that all WTTTs had a disk at some point of their evolution. It is possible that some disks dissipate very early ( $t \ll 1$  Myr), even before the star is optically revealed and can be classified as a WTT. However, accretion through a disk is considered an unavoidable step of the star formation process.

10 Myr. A related timescale is the transition timescale from optically thick accretion disks to undetectable disks. Assuming that WTTS disks are the link between CTTS disks and “diskless” WTTSs, then the transition timescale,  $\tau$ , can be estimated as  $\tau = (N_{\text{tran}}/N_{\text{PMS}})\langle \text{age} \rangle$ , where  $N_{\text{tran}}$  is the number of WTTS disks,  $N_{\text{PMS}}$  is the total number of PMS stars (WTTSs+CTTSs), and  $\langle \text{age} \rangle$  is the mean age of the sample. Adopting the WTTS/CTTS ratio of IC 348 ( $\sim 3/2$ ) and a mean age of 3 Myr, the overall IRAC disk fraction in WTTSs of 20% that we find in § 3.1 implies  $\tau \sim 0.4$  Myr. This timescale is very similar to that found for the transition timescale between an optically thick disk and an optically thin disk by Skrutskie et al. (1990) and Wolk & Walter (1996) based on the number of “transition objects,” which they define as targets without  $K$ -band excess but with strong *IRAS* excesses. The fact that the transitional timescale is significantly shorter than the mean disk lifetime is inconsistent with traditional viscous evolution (Hartmann et al. 1998) or magnetospheric clearing models (Armitage et al. 1999), which predict a steady disk evolution and thus similar timescales for disk lifetimes and disk dispersal times. Nonsteady disk evolution scenarios are required to explain the short transitional timescales inferred after significantly longer disk lifetimes. Such scenarios include the ultraviolet switch model (Alexander et al. 2006) and the presence of gap-forming planets (e.g., Quillen et al. 2004).

Our results from § 4.4 constrain not only the dissipation timescale of the dust during the planet formation process but also the amount of second-generation dust that is produced during this process (§ 4.3). Numerical models presented by Kenyon & Bromley (2004) predict the amount of 10 and 20  $\mu\text{m}$  excess as a function of time produced by the formation of terrestrial planets. Detailed comparison between these kinds of models with predictive power and the new observational constraints *Spitzer* is now providing could be highly valuable for our understanding of planet formation.

Particularly intriguing and potentially very important objects are the  $\sim 1$  Myr old WTTSs without any measurable IR excess (for  $\lambda \leq 24 \mu\text{m}$ ) discussed above. One possible explanation for the very early dissipation of their disks is that these stars have already formed planets through gravitational instability, which is expected to occur at extremely young ages when disks are most massive (Boss 2000). Another possibility for the fast dissipation of these disks is the presence of close companions that could have disrupted their disks. This possibility can be tested with a combination of radial velocity and adaptive optics observations to search for companions. Initial conditions could also be responsible for the early dissipation of the disk, although this hypothesis is not easily testable observationally. We note that the *Space Interferometry Mission PlanetQuest* should be able to establish whether or not these very young diskless WTTSs do in fact harbor planets. The presence of planets around these  $\sim 1$  Myr old stars would set the tightest constraints to date for the planet formation timescale.

The properties of WTTSs with disks such as their age, SED morphology,  $L_{\text{disk}}/L_*$ , etc., strongly suggest that WTTS disks are the link between the massive primordial disks found around CTTSs and the debris disks observed around young MS stars. They could be arguably the best places to study ongoing planet formation. Before the end of its mission, *Spitzer* is likely to identify hundreds of WTTS disks in nearby star-forming regions. These objects will most likely be the main targets of many follow-up observations. Deep far-IR and submillimeter observations with *Spitzer*, *Herschel Space Observatory*, and ALMA will allow the study of the outer regions of these WTTS disks and estimates of their masses. Follow-up *Spitzer* IRS observations of the 10 and 20  $\mu\text{m}$  silicate features will provide important information on the evolutionary

state of the circumstellar dust around these objects. Finally, high-resolution searches for  $\text{H}_2$  and atomic lines, such as those presented by Hollenbach et al. (2005) and Pascucci et al. (2006), would be highly desirable to constrain the amount of gas available for the formation of giant planets in WTTS disks.

## 5. SUMMARY OF RESULTS

We present a census of circumstellar disks and report the disk frequency as a function of stellar age for a sample of over 230 spectroscopically identified WTTSs located in the c2d IRAC and MIPS maps of the Ophiuchus, Lupus, and Perseus Molecular Clouds. Our main results can be summarized as follows:

1. In § 3.1 we find from a magnitude-limited subsample of WTTSs that  $\sim 20\%$  of the WTTSs have noticeable IR excesses at IRAC wavelengths indicating the presence of a circumstellar disk.

2. The disk frequencies we find in the three clouds we consider are  $\sim 3\text{--}6$  times larger than that recently found by P06 for a sample of 83 relatively isolated WTTSs projected outside the boundaries of nearby molecular clouds. This discrepancy in the disk fractions supports the idea that samples of WTTSs (nominally 1–10 Myr old) located a few degrees away from their parent molecular clouds represent an older population of stars. The disk fractions we find are more consistent with those obtained in recent *Spitzer* studies of WTTSs in young clusters such as IC 348 and Tr 37. However, in § 4.1.2 we suggest that Lada and colleagues might have overestimated the disk fraction of WTTSs in IC 348 by classifying as “anemic disks” some diskless M4–M7 stars with large photometric uncertainties.

3. In § 3.2.2 we find that the disk fraction of WTTSs is a smooth function of  $\text{H}\alpha$  EW. In § 3.2.4 we show that the fractional disk luminosities of WTTS disks bridge the gap between the CTTS and the debris disk range.

4. In § 4.3 we estimate mass upper limits of dust within the inner 10 AU of  $10^{-4} M_\oplus$  for the objects in our sample with 24  $\mu\text{m}$  fluxes consistent with stellar photospheres.

5. In § 4.4 we place our sample of WTTSs in the H-R diagram and find that the stars with excesses are among the younger part of the age distribution. However, we also find that up to  $\sim 50\%$  of the apparently youngest stars in the WTTS sample show no evidence of IR excess. This suggests that the circumstellar disks of a sizable fraction of PMS stars dissipate before the stars reach an age of  $\sim 1$  Myr.

6. Also in § 4.4, we find that none of the stars in our sample apparently older than  $\sim 10$  Myr have detectable circumstellar disks. Since *Spitzer* observations probe planet-forming regions of the disk ( $r \sim 0.1\text{--}10$  AU) and are capable of detecting IR excesses produced by very small amounts of dust, our results impose stronger constraints on the time available for the formation of planets than those provided by previous studies based on detections of disks in the near-IR.

7. Finally, in § 4.5 we estimate a transition timescale of  $\sim 0.4$  Myr between optically thick accretion disks and disks that are undetectable shortward of  $\sim 10 \mu\text{m}$ , in good agreement with previous results.

We thank the anonymous referee for his/her many detailed comments, which have helped to improve the paper. Support for this work, which is part of the Spitzer Legacy Science Program, was provided by NASA through contracts 1224608, 1230782, and 1230799 issued by the Jet Propulsion Laboratory, California Institute of Technology under NASA contract 1407. B. M. acknowledges the

Fundación Ramón Areces for financial support. Astrochemistry in Leiden is supported by an NWO Spinoza and NOVA grant and by the European Research Training Network “The Origin of Planetary Systems” (PLANETS, contract HPRN-CT-2002-00308). We thank the Lorentz Center in Leiden for hosting several meetings

that contributed to this paper. This publication makes use of data products from the Two Micron All Sky Survey, which is a joint project of the University of Massachusetts and the Infrared Processing and Analysis Center funded by NASA and the National Science Foundation. We also acknowledge use of the SIMBAD database.

## REFERENCES

- Alcalá, J. M., Krautter, J., Covino, E., Neuhaeuser, R., Schmitt, J. H. M., & Wichmann, R. 1997, *A&A*, 319, 184
- Alexander, R. D., Clarke, C. J., & Pringle, J. E. 2006, *MNRAS*, 369, 229
- Andrews, S., & Williams, J. 2005, *ApJ*, 631, 1134
- Armitage, P., Clarke, C., & Tout, C. 1999, *MNRAS*, 304, 425
- Augereau, J. C., & Beust, H. 2006, *A&A*, 455, 987
- Augereau, J. C., Lagrange, A., Mouillet, D., Papaloizou, J. C., & Grorod, P. 1999, *A&A*, 348, 557
- Backman, D. E., & Paresce, F. 1993, in *Protostars and Planets III*, ed. E. H. Levy & J. I. Lunine (Tucson: Univ. Arizona Press), 1253
- Beichman, C. A., et al. 2005, *ApJ*, 622, 1160
- Boss, A. 2000, *ApJ*, 536, L101
- Bouvier, J., & Appenzeller, I. 1992, *A&AS*, 92, 481
- Briceno, C., Hartmann, L. W., Stauffer, J. R., Gagne, M., Stern, R. A., & Caillault, J. P. 1997, *AJ*, 113, 740
- Calvet, N., D'Alessio, P., Hartmann, L., Wilner, D., Walsh, A., & Sitko, M. 2002, *ApJ*, 568, 1008
- Carpenter, J. M., Mamajek, E., Hillenbrand, L., & Meyer, M. 2006, *ApJ*, 651, L49
- Chen, C. H., et al. 2005, *ApJ*, 634, 1372
- Cieza, L. A., & Baliber, N. 2006, *ApJ*, 649, 862
- Cieza, L. A., Kessler-Silacci, J. E., Jaffé, D. T., Harvey, P. M., & Evans, N. J. 2005, *ApJ*, 635, 422
- Covino, E., Alcalá, J., Allain, S., Bouvier, J., Terranegra, L., & Krautter, J. 1997, *A&A*, 328, 187
- D'Alessio, P., Calvet, N., & Hartmann, L. 2001, *ApJ*, 553, 321
- D'Alessio, P., Calvet, N., Hartmann, L., Lizano, S., & Cantó, J. 1999, *ApJ*, 527, 893
- D'Alessio, P., et al. 2005, *ApJ*, 621, 461
- D'Antona, F., & Mazzitelli, I. 1994, *ApJS*, 90, 467
- . 1998, in *ASP Conf. Ser. 134, Brown Dwarfs and Extrasolar Planets*, ed. R. Rebolo, E. Martin, & M. R. Zapatero Osorio (San Francisco: ASP), 442 (DM98)
- de Geus, E. J., de Zeeuw, P. T., & Lub, J. 1989, *A&A*, 216, 44
- Dullemond, C. P., & Dominik, C. 2005, *A&A*, 434, 971
- Durisen, R. H., Boss, A. P., Mayer, L., Nelson, A. F., Quinn, T., & Rice, W. K. M. 2007, in *Protostars and Planets V*, ed. B. Reipurth, D. Jewitt, & K. Keil (Tucson: Univ. Arizona Press), 607
- Evans, N. J., II, et al. 2003, *PASP*, 115, 965
- . 2005, Third Delivery of Data from the c2d Legacy Project (Pasadena: Spitzer Science Center)
- Feigelson, E. D. 1996, *ApJ*, 468, 306
- Fiorucci, M., & Munari, U. 2003, *A&A*, 401, 781
- Furlan, E., et al. 2005, *ApJ*, 628, L65
- Haisch, K., Lada, E., & Lada, C. 2001, *ApJ*, 553, L153
- Hartigan, P., Edwards, S., & Ghadour, L. 1995, *ApJ*, 452, 736
- Hartigan, P., Strom, K., & Strom, S. 1994, *ApJ*, 427, 961
- Hartmann, L. 2001, *AJ*, 121, 1030
- Hartmann, L., Calvet, N., Gullbring, E., & D'Alessio, P. 1998, *ApJ*, 495, 385
- Hartmann, L., Megeath, S. T., Allen, L., Luhman, K., Calvet, N., D'Alessio, P., Franco-Hernandez, R., & Fazio, G. 2005, *ApJ*, 629, 881
- Harvey, P., et al. 2004, *BAAS*, 36, 726
- Hauschildt, P., Allard, F., & Baron, E. 1999, *ApJ*, 512, 377
- Herbig, G. H. 1998, *ApJ*, 497, 736
- Hillenbrand, L. A. 2002, preprint (astro-ph/0210520)
- . 2006, in *A Decade of Discovery: Planets around Other Stars*, ed. M. Livio (Baltimore: STScI), in press
- Hillenbrand, L. A., & White, R. J. 2004, *ApJ*, 604, 741
- Hollenbach, D., et al. 2005, *ApJ*, 631, 1180
- Hughes, J., Hartigan, P., Krautter, J., & Kelemen, J. 1994, *AJ*, 108, 1071
- Jorgensen, J. K., et al. 2006, *ApJ*, 645, 1246
- Kenyon, S. J., & Bromley, B. C. 2004, *ApJ*, 602, L133
- Kenyon, S. J., & Hartmann, L. 1995, *ApJS*, 101, 117
- Krautter, J., Wichmann, R., Schmitt, J. H. M. M., Alcalá, J. M., Neuhauser, R., & Terranegra, L. 1997, *A&AS*, 123, 329
- Lada, C. J., et al. 2006, *AJ*, 131, 1574 (L06)
- Lissauer, J., & Stevenson, D. L. 2007, in *Protostars and Planets V*, ed. B. Reipurth, D. Jewitt, & K. Keil (Tucson: Univ. Arizona Press), 591
- Liu, M., Matthews, B. C., Williams, J. P., & Kalas, P. G. 2004, *ApJ*, 608, 526
- Luhman, K., Stauffer, J., Muñch, A., Rieke, G., Lada, E., Bouvier, J., & Lada, C. 2003, *ApJ*, 593, 1093
- Mamajek, E. E., Meyer, M. R., & Liebert, J. 2002, *AJ*, 124, 1670
- Marcy, G. W., & Butler, R. P. 1998, *ARA&A*, 36, 57
- Martin, E. L. 1997, *A&A*, 321, 492
- Martin, E. L., & Magazzù, A. 1999, *A&A*, 342, 173
- Martin, E. L., Montmerle, T., Gregorio-Hetem, J., & Casanova, S. 1998, *MNRAS*, 300, 733
- Muzerolle, J., Calvet, N., Hartmann, L., & D'Alessio, P. 2003, *ApJ*, 597, L149
- Muzerolle, J., et al. 2006, *ApJ*, 643, 1003
- Osterloh, M., & Beckwith, S. V. 1995, *ApJ*, 439, 288
- Padgett, D. L., et al. 2006, *ApJ*, 645, 1283 (P06)
- Pascucci, I., et al. 2006, *ApJ*, 651, 1177
- Press, W. H., Teukolsky, S. A., Vetterling, W. T., & Flannery, B. P. 1992, *Numerical Recipes in C* (Cambridge: Cambridge Univ. Press)
- Quillen, A., Blackman, E., Frank, A., & Varnier, P. 2004, *ApJ*, 612, L137
- Richter, M. J., Jaffé, D. T., Blake, G. A., & Lacy, J. H. 2002, *ApJ*, 572, L161
- Schechter, P. L., Mateo, M., & Saha, A. 1993, *PASP*, 105, 1342
- Schneider, G., et al. 2006, *ApJ*, 650, 414
- Sicilia-Aguilar, A., et al. 2006, *ApJ*, 638, 897
- Siess, L., Dufour, E., & Forestini, M. 2000, *A&A*, 358, 593 (S00)
- Silverstone, M. D., et al. 2006, *ApJ*, 639, 1138
- Silvia, D. S. 1996, *A Bayesian Tutorial* (Oxford: Clarendon)
- Skrutskie, M. F., Dutkiewicz, D., Strom, S. E., Edwards, S., Strom, K. M., & Shure, M. A. 1990, *AJ*, 99, 1187
- Strom, K. M., Strom, S. E., Edwards, S., Cabrit, N., & Skrutskie, M. F. 1989, *AJ*, 97, 1451
- Strubbe, L. E., & Chiang, E. I. 2006, *ApJ*, 648, 652
- Thi, W. F., et al. 2001, *ApJ*, 561, 1074
- Weidenschilling, S. J. 1997, in *Proc. Lunar Planet. Sci. Conf.*, 28, 1517
- Weingartner, J. C., & Draine, B. T. 2001, *ApJ*, 548, 296
- Wichmann, R., Krautter, J., Covino, E., Alcalá, J. M., Neuhauser, R., & Schmitt, J. H. M. 1997, *A&A*, 320, 185
- Wichmann, R., et al. 2000, *A&A*, 359, 181
- White, R., & Basri, G. 2003, *ApJ*, 582, 1109
- Wolk, S. J., & Walter, F. M. 1996, *AJ*, 111, 2066
- Young, K. E., et al. 2005, *ApJ*, 628, 283